Cell Reports

Resource

A multimodal screening platform for endogenous dipeptide repeat proteins in *C9orf72* patient iPSC neurons

Graphical abstract

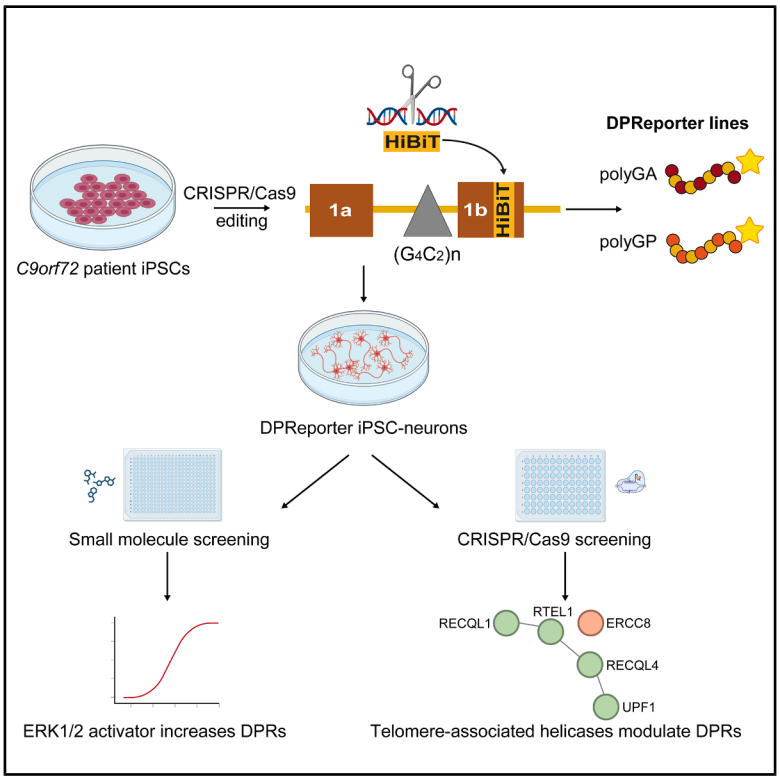

Highlights

- "DPReporter" lines allow sensitive and rapid DPR detection in lysed and live cells
- Amenable to high-throughput genetic and small-molecule screening
- Small-molecule screen showed ERK1/2 activator periplocin inhibits DPR turnover
- CRISPR screen reveals modulation of DPR levels by telomere-associated helicases

Authors

Benedikt V. Hölbling, Yashica Gupta, Paolo M. Marchi, ..., Emma Armstrong, Paul Whiting, Adrian M. Isaacs

Correspondence

a.isaacs@ucl.ac.uk

In brief

Hölbling et al. generate "DPReporter" iPSC neuron lines, which report the levels of endogenous dipeptide repeat proteins (DPRs) generated by the frontotemporal dementia and amyotrophic lateral sclerosis-causing repeat expansion in *C9orf72*. Their utility for small-molecule and CRISPR-Cas9 screening was demonstrated, thus providing a powerful resource for repeat expansion disease research.

Hölbling et al., 2025, Cell Reports *44*, 115695
May 27, 2025
https://doi.org/10.1016/j.celrep.2025.115695

CellPress

Cell Reports

CellPress
OPEN ACCESS

Resource

A multimodal screening platform for endogenous dipeptide repeat proteins in *C9orf72* patient iPSC neurons

Benedikt V. Hölbling,[1,2,14] Yashica Gupta,[1,2,14] Paolo M. Marchi,[1,2,14] Magda L. Atilano,[3] Michael Flower,[1,2] Enric Ureña,[3] Rajkumar A. Goulden,[3] Hannah K. Dobbs,[1,2] Eszter Katona,[1,2] Alla Mikheenko,[2,4] Ashling Giblin,[1,2,3] Ali Raza Awan,[5,6] Chloe L. Fisher-Ward,[5] Niamh O'Brien,[7,8] Deniz Vaizoglu,[1,2] Liam Kempthorne,[1,2] Katherine M. Wilson,[1,2] Lauren M. Gittings,[1,2,13] Mireia Carcolé,[1,2] Marc-David Ruepp,[7,8] Sarah Mizielinska,[7,8] Linda Partridge,[3] Pietro Fratta,[4,9] Sarah J. Tabrizi,[1,2] Bhuvaneish T. Selvaraj,[10,11] Siddharthan Chandran,[10,11] Emma Armstrong,[12] Paul Whiting,[2,12] and Adrian M. Isaacs[1,2,15,*]

[1]Department of Neurodegenerative Disease, UCL Queen Square Institute of Neurology, London, UK
[2]UK Dementia Research Institute at UCL, London, UK
[3]Institute of Healthy Ageing, Department of Genetics, Evolution and Environment, UCL, London, UK
[4]Department of Neuromuscular Diseases, UCL Queen Square Institute of Neurology, London, UK
[5]Genomics Innovation Unit, Guy's and St Thomas' NHS Trust, London, UK
[6]Comprehensive Cancer Centre, King's College London, London, UK
[7]UK Dementia Research Institute at King's College London, London, UK
[8]Department of Basic and Clinical Neuroscience, Institute of Psychiatry, Psychology & Neuroscience, King's College London, London, UK
[9]The Francis Crick Institute, London, UK
[10]UK Dementia Research Institute at University of Edinburgh, Edinburgh, UK
[11]Centre for Clinical Brain Sciences, University of Edinburgh, Edinburgh, UK
[12]Alzheimer's Research UK Drug Discovery Institute, UCL, London, UK
[13]Present address: Barrow Neurological Institute, Phoenix, AZ, USA
[14]These authors contributed equally
[15]Lead contact
*Correspondence: a.isaacs@ucl.ac.uk
https://doi.org/10.1016/j.celrep.2025.115695

SUMMARY

Repeat expansions in *C9orf72* are the most common cause of amyotrophic lateral sclerosis and frontotemporal dementia. Repeat-associated non-AUG (RAN) translation generates neurotoxic dipeptide repeat proteins (DPRs). To study endogenous DPRs, we inserted the minimal HiBiT luciferase reporter downstream of sense repeat derived DPRs polyGA or polyGP in *C9orf72* patient iPSCs. We show these "DPReporter" lines sensitively and rapidly report DPR levels in lysed and live cells and optimize screening in iPSC neurons. Small-molecule screening showed the ERK1/2 activator periplocin dose dependently increases DPR levels. Consistent with this, ERK1/2 inhibition reduced DPR levels and prolonged survival in *C9orf72* repeat expansion flies. CRISPR knockout screening of all human helicases revealed telomere-associated helicases modulate DPR expression, suggesting common regulation of telomeric and *C9orf72* repeats. These DPReporter lines allow investigation of DPRs in their endogenous context and provide a template for studying endogenous RAN-translated proteins, at scale, in other repeat expansion disorders.

INTRODUCTION

Expansions of short tandem repeats are associated with several neurodegenerative and neuromuscular diseases, including amyotrophic lateral sclerosis (ALS) and frontotemporal dementia (FTD),[1,2] fragile X-associated tremor/ataxia syndrome (FXTAS),[3] myotonic dystrophy type 1 and 2 (DM1, DM2),[4,5] and Huntington's disease.[6] These repeat expansion disorders vary considerably in disease mechanisms, clinical presentation, repeat length, and location within the genome.[7] However, one feature shared by several of these diseases is the generation of repetitive proteins encoded by the repeat expansion through an unconventional process known as repeat-associated non-AUG (RAN) translation. Thus, understanding the mechanisms underlying the generation and degradation of these repetitive proteins may provide novel insights and yield new therapeutic approaches for repeat expansion diseases. Large-scale genetic and small-molecule screening holds great potential for providing such insights but has been challenging to achieve in physiological systems such as patient-derived cells. Here, we focused on the repeat expansion in *C9orf72* in order to overcome these challenges and develop a multimodal screening platform in patient iPSC neurons.

A G_4C_2 hexanucleotide repeat expansion in intron 1 of the *C9orf72* gene is the most common genetic cause of ALS and FTD.[1,2] The repeat expansion is translated in all reading frames via RAN translation to generate five distinct dipeptide repeat proteins (DPRs), which accumulate in CNS tissue.[8–13] PolyGA, polyGP, and polyGR are translated from the sense (GGGGCC)n RNA and polyGP, polyAP, and polyPR are translated from the antisense (GGCCCC)n RNA. The arginine-rich DPRs, polyGR and polyPR, exhibit strong neural toxicity *in vivo* and *in vitro,*[14–17] with polyGA also able to cause toxicity.[17–19] Current evidence suggests that a near-cognate CUG start codon initiates translation of polyGA and potentially other sense-derived DPRs.[20–24] In addition, genetic screening has provided further insight into the regulation of DPR RAN translation. For example, the loss of DEAH-box helicase 36 (*DHX36*) and small ribosomal protein subunit 25 (*RPS25*) causes a reduction in DPR levels, classifying them as RAN translation enhancers.[25–27] In contrast, overexpression of the DEAD-box helicase 3 X-linked (*DDX3X*) inhibits *C9orf72* RAN translation, classifying it as an inhibitor of *C9orf72* repeat RAN translation; however, it has the opposite effect on CGG-repeats in the *FMR1* gene, where it enhances RAN translation.[28–31]

Notably, these genetic screening studies utilized overexpression of GGGGCC repeat constructs that are shorter than the repeat expansions typically found in affected individuals and do not recapitulate the full *C9orf72* locus sequence and associated regulatory elements. Therefore, screening of DPRs in their endogenous context is needed to fully understand the mechanisms underlying DPR expression and degradation. As DPRs are most highly expressed in neurons and can cause cell-autonomous neuronal toxicity, patient-derived iPSC neurons are an ideal system to study DPR regulation. However, detection of endogenous DPRs is limited by low expression levels, hampering the ability to perform high-throughput screening assays. Currently, antibody-based detection methods such as Meso Scale discovery (MSD) and Simoa immunoassays are required for sensitive and specific DPR quantification but are challenging to use in high-throughput screening workflows.[32–35] We therefore developed an approach that allows high-throughput genetic and small-molecule screening of endogenous *C9orf72* DPR levels in iPSC neurons, and which can be applied to other repeat expansion disorders in the future. We demonstrate the utility of this system for both CRISPR-based and small-molecule screening in iPSC neurons to identify modulators of DPR expression and turnover.

RESULTS

Generation of *C9orf72* patient i^{3}N DPReporter lines

As our goal was to generate lines amenable to screening in iPSC neurons, we first generated a *C9orf72* patient i^{3}N line. The i^{3}N system introduces an inducible neurogenin 2 (NGN2) expression cassette to allow rapid and scalable differentiation into glutamatergic neurons.[36,37] To generate a *C9orf72* patient i^{3}N parental line, we used CRISPR-Cas9 to integrate a cassette encoding the fluorescent reporter NLS-mApple and doxycycline-inducible neurogenin 2 (NGN2) into the CLYBL safe harbor locus of a patient line harboring ~700 repeats (Figure S1A). We confirmed the expected rapid neuronal differentiation after doxycycline addition, with >95% of cells expressing the neuronal marker microtubule-associated protein 2 (Map2), neuron-specific class III β-tubulin (TuJ1), $GABA_A$ receptor, and AMPA receptor subunit GluR2, but not pluripotency marker SRY-box2 (SOX2) after 5 days of differentiation (Figures S1B and S1C).

To detect endogenous DPRs generated from the complete *C9orf72* genomic locus, we next used CRISPR-Cas9 to insert the small, sensitive HiBiT tag downstream of the GGGGCC repeat expansion into either the polyGA or polyGP frames in our i^{3}N patient line (Figure 1A), to generate "DPReporter" lines. We focused on these DPR species as in our experience they are robustly detected in patient iPSC neurons using MSD immunoassay,[38,39] whereas we are unable to detect polyGR in iPSC neurons using the same MSD immunoassay approach (Figure S1D). Genome editing was designed to ensure the absence of intervening stop codons between the repeats and the tag. We confirmed integration into the repeat-containing allele by association of the HiBiT tag with the expanded repeat-linked SNP rs10757668 (Figure S1E) and sequencing of the 3′ end of HiBiT confirmed integration into the endogenous *C9orf72* locus (Figure S1F). Measurement of *C9orf72* RNA and protein levels showed a significant decrease in C9orf72 protein levels in our favored i^{3}N GA-HiBiT line (Figures S1G–S1I), but as the C9orf72 protein was still visibly present and it passed all other criteria it was taken forward for further testing.

Measurement of polyGA-HiBiT and polyGP-HiBiT in day 5 neurons using the Nano-Glo lytic luciferase assay in the i^{3}N GA-HiBiT and i^{3}N GP-HiBiT lines exceeded the background levels of the untagged i^{3}N C9 parental line by 130- and 20-fold, respectively (Figure 1B). We also analyzed a line in which the HiBiT tag had only been inserted into the unexpanded allele. As expected, this line showed minimal luminescence signal (Figure 1C), confirming that the luminescence signal we observe in our DPReporter lines is due to RAN translation of HiBiT from the expanded allele. To further validate the specificity of the luciferase signal, we treated our i^{3}N DPReporter lines with an antisense oligonucleotide (ASO) targeting *C9orf72* intron 1.[40] The C9-ASO reduced polyGA-HiBiT and polyGP-HiBiT levels in both DPReporter lines in the luciferase assay (Figure 1D) and MSD immunoassay (Figure 1E) to the same extent, indicating the luminescence signal we observe is derived from HiBiT-tagged DPRs.

We next investigated whether the HiBiT tag could be used to detect endogenous DPRs in live iPSC neurons. We transfected a plasmid encoding the LgBiT luciferase component into the i^{3}N C9 parental, i^{3}N GA-HiBiT, and i^{3}N GP-HiBiT lines simultaneously with the initiation of neuronal induction. On day 3 of differentiation, polyGP-HiBiT and polyGA-HiBiT were successfully detected by live luminescence reading only in LgBiT-transfected DPReporter iPSC neurons, but not control wells (Figures S1J and S1K). Overall, these data show that our i^{3}N DPReporter lines can sensitively, robustly, and rapidly detect endogenous DPRs in both lysed and live cells.

We also generated HiBiT tagged versions of our *C9orf72* patient parental line without the NGN2 cassette using a similar workflow (Figure S2). We then performed a more detailed analysis of our selected DPReporter lines. We measured the levels of *C9orf72* sense and antisense repeat RNA foci, which we

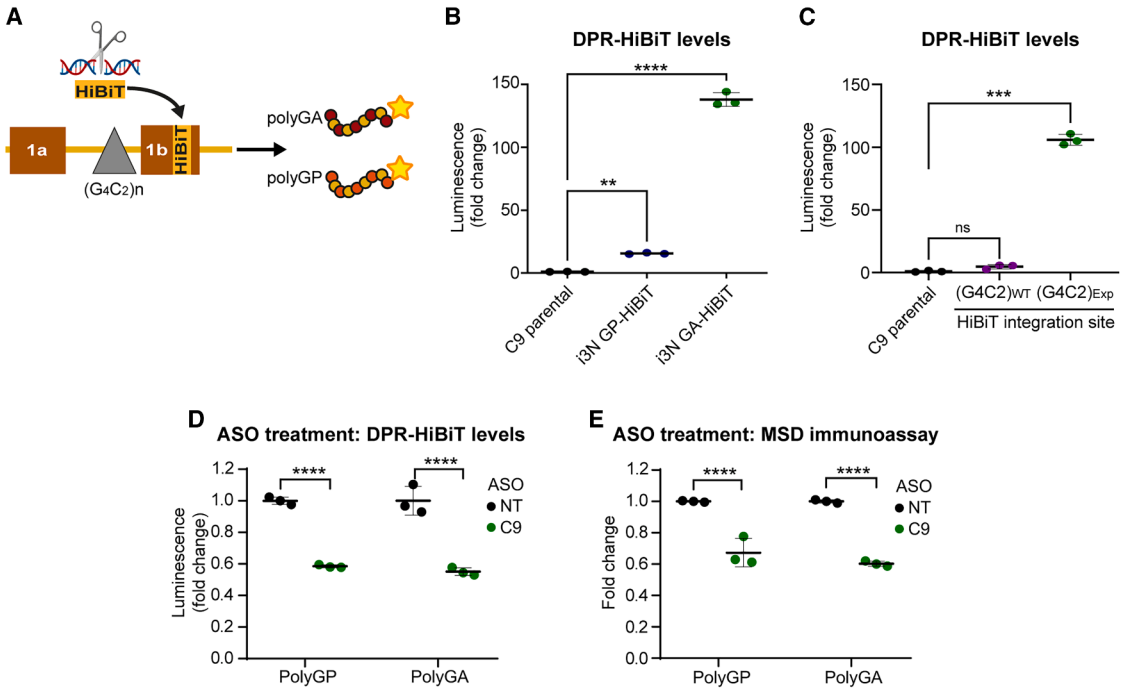

Figure 1. Generation of *C9orf72* patient iPSC endogenous DPR reporter lines

(A) The 11 amino acid HiBiT tag, followed by a stop codon, was inserted using CRISPR-Cas9 into *C9orf72* exon 1b in either polyGA or polyGP frames to generate "DPReporter" cell lines.

(B) Detection of HiBiT luminescence in differentiated DPReporter cells reveals sensitive detection of endogenous DPRs with 20- to 130-fold signal-to-noise ratio when compared with the untagged parental line (**$p \leq 0.01$, ****$p \leq 0.0001$, one-way ANOVA, $N = 3$ inductions).

(C) DPR-HiBiT levels are exclusively detected from tagging of the expanded *C9orf72* allele (G4C2)Exp, with no signal from insertion into the unexpanded wild-type (WT) allele (***$p \leq 0.001$, one-way ANOVA, $N = 3$ inductions).

(D and E) Signal specificity was confirmed by treatment with an ASO targeting *C9orf72* intron 1. After 3 days, DPR-HiBiT luminescence signal and MSD immunoassay signal were reduced to the same extent, compared with a non-targeting control (NT) ASO (****$p < 0.0001$, t test, $N = 3$ inductions). Data are presented as mean ± SD.

specifically detect in *C9orf72* patient lines (Figures S3A–S3G), antisense RNA transcripts (Figure S3H), and expression of pluripotency markers (Figure S4) and observed small increases in sense RNA foci in a subset of lines but otherwise no differences between the original *C9orf72* parental line and all subsequently derived lines. As the HiBiT tag is inserted at the 3′ end of non-coding exon 1b, we also measured the ratio of exon 1a and exon 1b usage and found no change as compared with the parental line, except for the non-i^{3}N GP-HiBiT line, which had an increased ratio of exon 1b to exon 1a usage (Figure S5). Genomic integrity was first assessed by qPCR analysis for common karyotypic abnormalities and sequencing of predicted potential CRISPR off-target sites (Figures S6A–S6L), which showed no alterations in the i^{3}N DPReporter lines. A broader karyotype analysis across all our lines was then performed using KaryoStat+ genome-wide comparative genome hybridization, which has a higher resolution than standard G-banding. Either one or two microduplications that were too small for detection by G-banding were identified in all lines (Figure S7), indicating they were not due to genome editing. We next performed Southern blotting to ascertain repeat length (Figures S8A and S8B). The parental line showed a smear from approximately 400 to 800 repeats and all the edited lines fell within this range except the non-i^{3}N GA-HiBiT DPReporter line, which had a contraction to approximately 200 repeats. For further validation, we performed targeted adaptive Oxford Nanopore Technology (ONT) long-read sequencing. The use of targeted ONT sequencing provided high read depth (55–150 reads across the repeat), allowing robust repeat sizing, which was consistent with Southern blotting (Figure S8C). However, the fidelity of reads through the repeat sequence was not sufficient for us to confirm whether the HiBiT tag had integrated into the correct DPR frame. We therefore performed PacBio long-read sequencing, which provided enhanced fidelity across the repeat sequence, and confirmed the expected position of the HiBiT tag downstream of the expanded repeat (Figure 2). Although predicting the frame with 100% confidence is not possible as just a single base pair error over the extensive repeat will alter the frame, the enhanced fidelity gave us confidence to predict the frame, especially at the 3′ end of the repeat reading into the HiBiT tag. This showed that our i^{3}N and non-i^{3}N GA and GP reporter lines were predicted to have the HiBiT tag in their respective frames (Figures S9A and S9B). The long-read sequencing also confirmed our short-read sequencing (Figure S1F), which showed correct insertion of HiBiT at the 3′ insertion site (Figure S9). The long-read sequencing additionally showed the 5′ insertion site, which we were unable

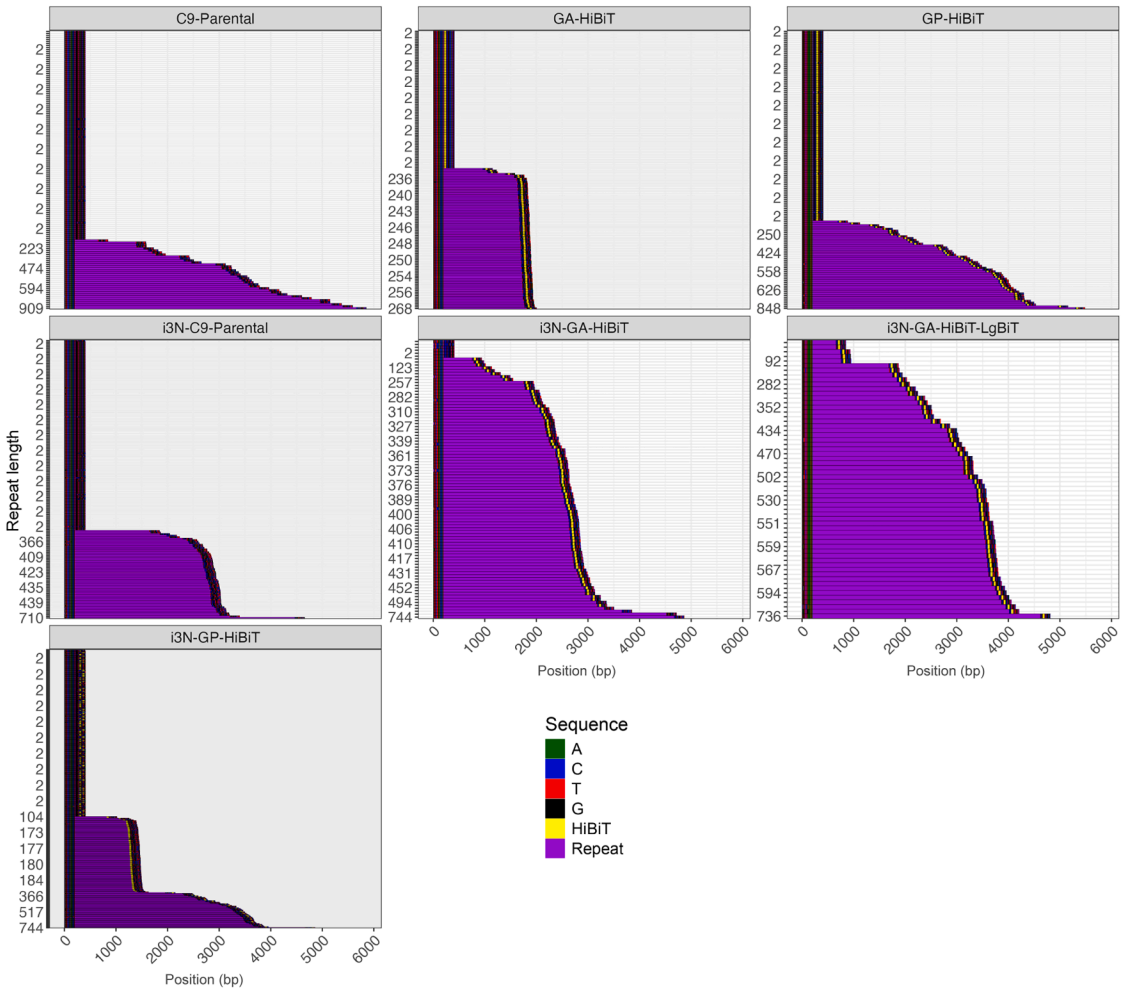

Figure 2. Waterfall plots showing repeat length and HiBiT insertion in the DPReporter iPSC lines

PacBio PureTarget long-read *C9orf72* sequences were trimmed to 200 bases flanking the hexanucleotide repeat. Each row represents a read, with the *x* axis indicating base position along the read and the *y* axis giving hexanucleotide repeat length. Each base position is colored according to the legend, with the hexanucleotide repeat highlighted purple and HiBiT tag yellow.

to interrogate with short-read sequencing due to the high GC content and proximity to the repeat sequence. This revealed that the GA-HiBiT, GP-HiBiT, and i^{3}N GP-HiBiT lines had small deletions or duplications of exon 1b at the 5′ insertion site (Figure S9B) and HiBiT insertion into the wild-type allele, also with small deletions at the 5′ insertion site (Figure S9C). However, our i^{3}N GA-HiBiT line showed clean insertion of the HiBiT tag at both 5′ and 3′ insertion sites and no insertion into the wild-type allele (Figures S9B and S9C). We therefore took this line forward for screening and kept the other lines for validation experiments.

Utilization of i^{3}N DPReporter lines for high-throughput small-molecule screening

To determine the utility of the i^{3}N DPReporter system for high-throughput screening, we optimized culture conditions and luminescence detection in 384-well format (Figure 3A). We used *C9orf72* ASO treatment to confirm that reduced DPR-HiBiT levels could be robustly detected in i^{3}N GA-HiBiT neurons after 72 h with favorable screening parameters (CV_{CTRL} = 6.6, CV_{C9} = 4.9, Z' = 0.75) (Figure S10A). To enhance utility for high-throughput screening, we optimized multiplexing the luciferase assay with a fluorescence-based toxicity assay, which did not interfere with DPR detection (Figure S10B). To further confirm the suitability of our reporter line to identify small-molecule modifiers of DPR levels, we treated i^{3}N GA-HiBiT neurons with the nucleoside analog decitabine, as it has previously been shown to reduce DPR levels in *C9orf72* patient iPSC neurons.[35] Decitabine reduced polyGA-HiBiT levels in a dose-dependent manner, confirming that the HiBiT tag had not interfered with the ability to detect DPR modulators (Figure 3B). We next performed a proof-of-concept high-throughput screen of a natural product library comprising 1,444 compounds. While these compounds are relatively unselective and unlikely to yield candidates for drug development, they allow testing and validation of the assay for high-throughput screening.

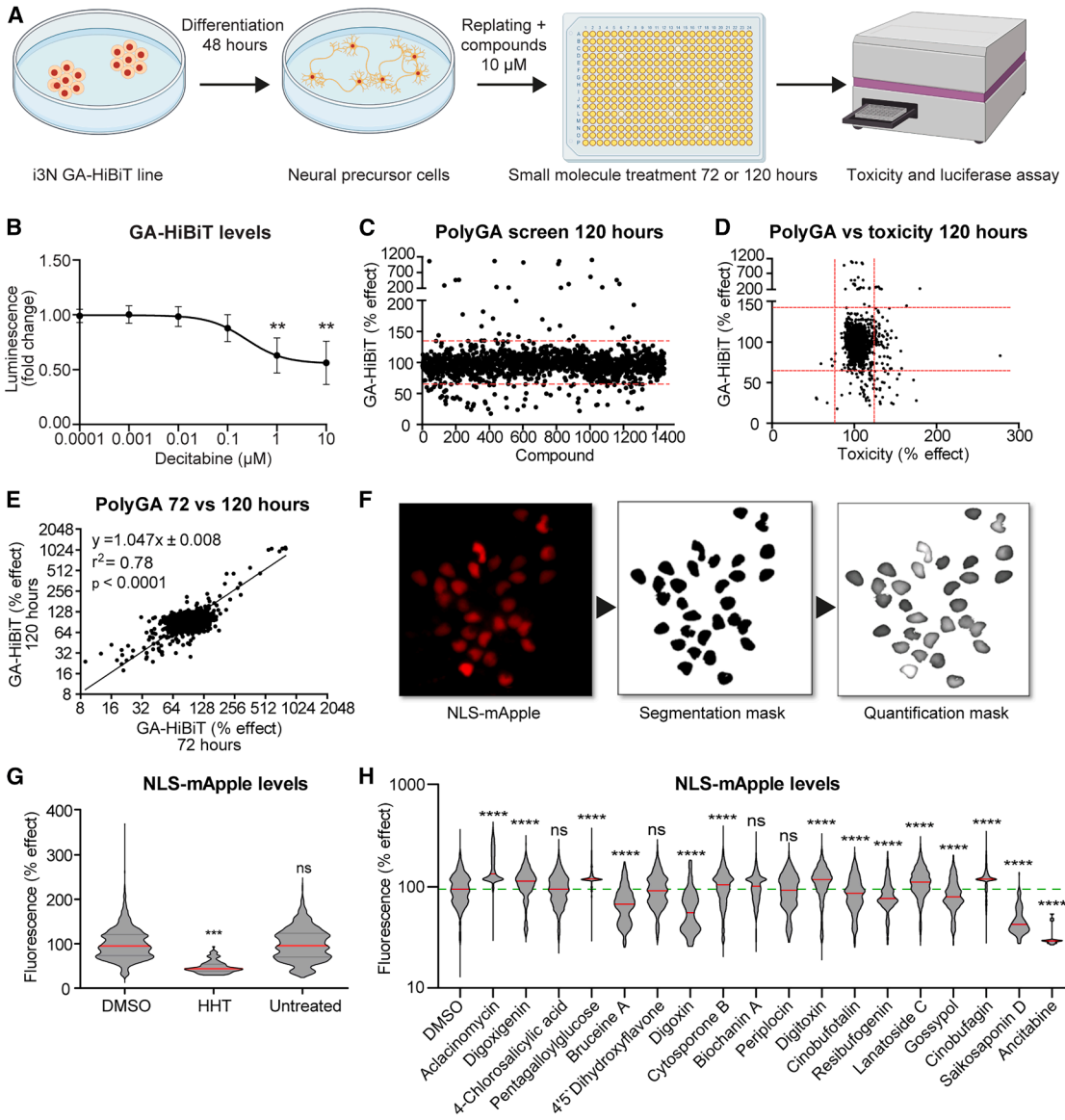

Figure 3. Small-molecule high-throughput screening of endogenous DPR levels in i^{3}N DPReporter iPSC neurons

(A) Schematic representation of HTS workflow. DPReporter iPSCs are induced for 48 h before replating on 384-well small-molecule library plates (10 µM). Cells were cultured for 72 or 120 h before determining compound toxicity and polyGA-HiBiT levels.

(B) PolyGA-HiBiT levels are dose dependently decreased by treatment with decitabine (N = 3 inductions, mean ± SD, $^{**}p \leq 0.01$, one-way ANOVA).

(C) PolyGA-HiBiT levels after 120-h treatment determined by HiBiT assay (red lines = mean ± 3×SD window of DMSO treated control wells).

(D) Comparison of compound toxicity and effect on polyGA-HiBiT levels after 120 h (red lines = mean ± 3×SD window of DMSO-treated control wells).

(E) Correlation of hit compounds from 72- and 120-h treatment (linear regression).

(F) Nuclear mApple fluorescence intensity is quantified by a semi-automated image analysis pipeline.

(G) Canonical translation levels are reduced upon treatment with translation inhibitor homoharringtonine (HHT), but not DMSO ($^{***}p \leq 0.001$, ANOVA).

(H) Quantification of NLS-mApple canonical translation reporter expression for the top 18 compounds (10 µM) that modified polyGA-HiBiT levels in the primary screen ($^{****}p \leq 0.0001$, one-way ANOVA, green line = DMSO median). Data are presented as median unless stated otherwise.

Screens were performed with compounds at 10 µM final concentration for either 120 h (Figures 3C and S10C) or 72 h (Figures S10D–S10E) at 37°C. The multiplexed cell toxicity assay (Figures 3D and S10F) enabled exclusion of toxic compounds, followed by luminescence detection to identify hit compounds. The entire screening workflow for 1,444 compounds took <1 h and showed robust screening parameters (CV_{DMSO} = 12). Hit compounds were defined by polyGA-HiBiT levels 3×SD below or above the DMSO-treated control wells, identifying 25 hit compounds that decreased DPR levels and 31 compounds that increased DPR levels, without causing toxicity. Encouragingly, hits from the 72- and 120-h treatments showed a very high

correlation (r^2 = 0.78, p < 0.0001) (Figure 3E), confirming the reproducibility of the assay.

To determine compound specificity for DPR expression over global gene expression, fluorescence intensity of the canonically translated NLS-mApple reporter was quantified using a semi-automated image analysis pipeline (Figures 3F and S10G). Inhibiting canonical translation by treatment with 10 μM homoharringtonine significantly reduced mApple levels compared with DMSO and untreated controls (Figure 3G), confirming the ability of the assay to identify general inhibitors of translation. Reduction of DPR levels by ASO treatment did not affect mApple reporter expression (Figures S10H and S10I) indicating that endogenous DPRs are not affecting canonical translation over the period of the assay. Thus, modulation of DPR levels by the compounds screened will not affect interpretation of the results. Next, the effects of the 18 strongest DPR expression enhancers and inhibitors on canonical translation were determined. Fourteen compounds affected mApple expression levels, while four compounds (three inhibitors and one enhancer) did not and thus specifically altered polyGA-HiBiT levels (Figure 3H). Structural characterization of the remaining three DPR inhibitors (biochanin A, 4-5-dihydroxyflavone, 4-chlorosalycylic acid) identified them as pan-assay interference compounds, so were subsequently excluded from further analysis.[41] In contrast, the DPR expression enhancer, periplocin, belongs to the cardiac glycosides, which do not possess described assay-interfering characteristics.[42] Periplocin increased polyGA-HiBiT and polyGP-HiBiT levels in a concentration-dependent manner in the i^3N DPReporter lines (EC_{50} = 0.4 μM) (Figures 4A and S11A). Importantly, effects were confirmed by MSD immunoassay in three unedited patient iPSC-derived lines (Figure 4B), confirming that the effect is not related to the HiBiT tag. Overall, these results validate the capability of the DPReporter platform to perform high-throughput small-molecule screening and identify periplocin as an enhancer of endogenous polyGA and polyGP levels.

Small-molecule periplocin slows DPR turnover via ERK1/2 activation

To determine how periplocin affects DPR levels, we developed a live-labeling protocol for endogenous DPRs in living cells to track their degradation over time using HiBiT luminescence (Figure 4C). We introduced a Tet-ON-LgBiT cassette into the polyGA-HiBiT i^3N DPReporter cell line to gain temporal control of LgBiT expression. These DPReporter iPSCs were treated with doxycycline to simultaneously induce both NPC differentiation and LgBiT expression to allow subsequent LgBiT labeling of HiBiT-tagged endogenous DPRs. After the removal of doxycycline, only LgBiT-labeled DPRs will emit a luminescent signal when assayed while newly generated, unlabeled DPRs remain undetected. Consequently, luminescence directly correlates to levels of initially labeled DPRs and enables quantification of DPR turnover. While endogenous polyGA-HiBiT levels decreased by ~85% after 72 h, there was no decline in polyGA-HiBiT levels over the same period with periplocin treatment (Figure 4D), showing that periplocin inhibits DPR turnover ($t_{1/2}$DMSO = 36 h, $t_{1/2}$ periplocin > 96 h). Periplocin also slowed polyGP-HiBiT turnover using the live labeling protocol in the i^3N GP-HiBiT cell line (Figure S11B). *C9orf72* RNA transcript levels were unaffected by periplocin treatment (Figures S11C–S11E), but interestingly we observed a small decrease in both sense and antisense RNA foci in the i^3N GA-HiBiT and untagged parental line after periplocin treatment (Figures S11F–S11I). This indicates that periplocin could be acting at the RNA level in addition to reducing DPR protein turnover. These results demonstrate the utility of our DPR live labeling assay to track the turnover of endogenous DPRs and show that one action of periplocin is to slow DPR turnover.

To further interrogate the mechanism of action of periplocin we investigated its reported roles as an inhibitor of the unfolded protein response (UPR),[42] and as an activator of the ERK1/2 and AMP kinases.[43] We first investigated the UPR, which consists of three distinct pathways, IRE1-XBP1, ATF6, and eIF2α (Figure S12A).[44] Periplocin treatment reduced levels of the spliced/activated isoform of XBP1 (Figures S12B and S12C), showing that the IRE1-XBP1 axis is inhibited upon periplocin treatment in i^3Neurons. In contrast, periplocin did not affect the ratio of phosphorylated eIF2α to total eIF2α protein (Figure S12D), and inhibition of the ATF6 pathway with the specific inhibitor ceapin (5 μM, IC_{50} = 0.5 μM)[45] did not result in increased polyGA or polyGP levels in HiBiT assays conducted on the i^3N GA-HiBiT and i^3N GP-HiBiT lines, nor in MSD assays of three unedited patient iPSC-derived lines (Figures S12E and S12F). To determine whether periplocin's effect on IRE1-XBP1 is driving the increase in DPRs we used an orthogonal approach by knocking out *ERN1*, which encodes IRE1, in i^3N GA-HiBiT neurons using CRISPR-Cas9 (Figure S12G). We achieved effective reduction of *ERN1* mRNA (Figures S12H and S12I), which reduced spliced XBP1 transcript levels to a similar extent to periplocin (Figure S12J); however, polyGA-HiBiT levels were not altered (Figure S12K). These experiments rule out an effect of periplocin on DPRs via the IRE1 arm of the UPR.

We therefore next assessed the effect of periplocin on ERK1/2 and AMPK activation. Periplocin had no effect on total AMPK levels (Figures S12L and S12M) or AMPK phosphorylation, which was undetectable in our i^3N GA-HiBiT line. In contrast, periplocin dose dependently increased the ratio of phosphorylated ERK1/2 to total ERK1/2 (Figures 4E and 4F). ERK1/2 are directly activated by MEK1/2 kinase and can be inhibited by MEK1/2 antagonists.[46] Therefore, to determine whether periplocin's activation of the ERK1/2 pathway is responsible for driving its effect on DPRs, we pre-treated i^3N GA-HiBiT neurons with the MEK1/2 inhibitor trametinib, followed by our standard 3-day periplocin treatment. Trametinib abrogated periplocin's activation of ERK1/2 phosphorylation (Figures 4G and 4H) and partially inhibited its effect on DPR levels (Figure 4I), indicating that periplocin may be acting in part via ERK1/2 activation to increase DPR levels.

Next, to investigate this pathway in a different model system, we used our established *C9orf72 Drosophila* model, which expresses 36 GGGGCC repeats under the control of an inducible neuron-specific driver and causes dramatically shortened lifespan.[17] Consistent with the data from our DPReporter neurons, trametinib treatment reduced both ERK phosphorylation and polyGP levels in adult *C9orf72* repeat fly

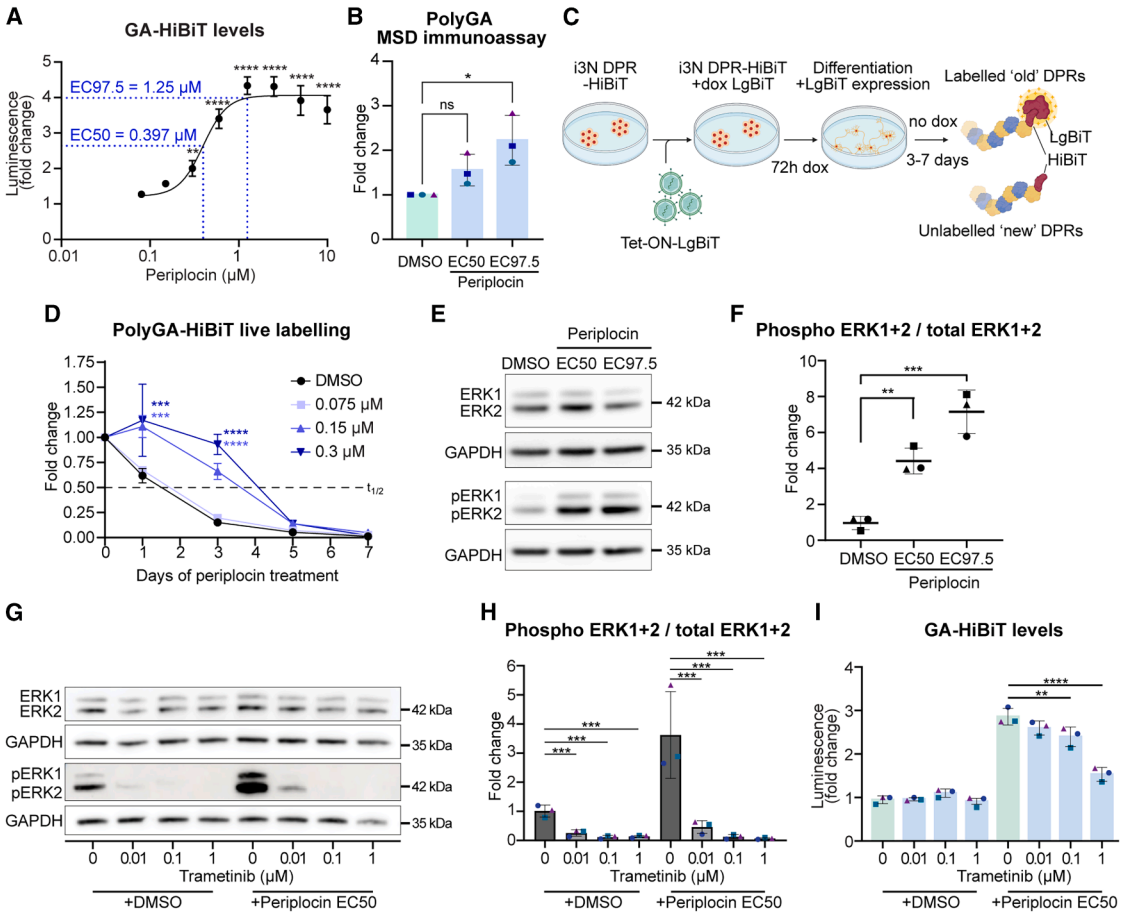

Figure 4. Unfolded protein response inhibitor periplocin reduces DPR turnover through activation of ERK1/2

(A) Concentration-dependent increase in endogenous polyGA-HiBiT levels upon periplocin treatment for 3 days in the DPR-HiBiT assay (presented as fold change over DMSO control, $^{**}p \leq 0.01$, $^{****}p \leq 0.0001$, one-way ANOVA, $N = 3$ inductions). Half-maximal effective concentration (EC_{50}) is 0.397 µM (non-linear regression).

(B) Endogenous polyGA levels after 3 days of periplocin treatment at EC_{50} (0.397 µM) and $EC_{97.5}$ (1.25 µM) in neurons of 3 independent patient iPSC lines, measured by MSD immunoassay ($^{*}p \leq 0.05$, one-way ANOVA, $N = 3$ unedited cell lines).

(C) Overview of live-DPR labeling protocol: a doxycycline-inducible LgBiT expression cassette was introduced in i^3N DPR-reporter cells by lentiviral transduction. Cells are induced into neural progenitor cells by doxycycline treatment while simultaneously triggering LgBiT expression for labeling of DPR-HiBiT proteins. After baseline luminescence detection (0 h), cells are treated in absence of doxycycline to determine reduction of labeled DPRs over time.

(D) Live labeling of endogenous polyGA-HiBiT enables determination of turnover. Degradation of endogenous polyGA-HiBiT is slowed by periplocin treatment ($^{***}p \leq 0.001$, $^{****}p \leq 0.0001$, two-way repeated measures ANOVA, $N = 3$ inductions).

(E and F) (E) Western blot and (F) quantification of the phosphorylated to total ERK1/ERK2 ratio in i^3N GA-HiBiT neurons after 3 days of treatment with periplocin at EC_{50} (0.397 µM) and $EC_{97.5}$ (1.25 µM) doses ($^{**}p \leq 0.01$, $^{***}p \leq 0.001$, one-way ANOVA, $N = 3$ inductions).

(G and H) (G) Western blot and (H) quantification of the phosphorylated to total ERK1/ERK2 ratio in i^3N GA-HiBiT neurons after 6 days of treatment with the MEK1/2 inhibitor trametinib (0, 0.01, 0.1, 1 µM), followed by an additional 3 days in combination with either DMSO or the EC_{50} dose of periplocin ($^{***}p \leq 0.001$, one-way ANOVA, $N = 3$ inductions).

(I) Quantification of polyGA-HiBiT luminescence under the same experimental conditions as described in (G) and (H) ($^{**}p \leq 0.01$, $^{***}p \leq 0.001$, one-way ANOVA, $N = 3$ inductions). Data are presented as mean ± SD unless indicated otherwise.

heads (Figures 5A–5D). Trametinib treatment was also sufficient to significantly extend the lifespan of our *C9orf72* repeat flies (Figure 5E), with an even stronger effect when the adult flies were pre-treated with trametinib for 7 days prior to inducing expression of the *C9orf72* repeats (Figure 5F). These data confirm that the findings made in our DPReporter lines translate to other model systems and show that modulating ERK1/2 activation alters DPR levels *in vitro* and *in vivo*.

CRISPRn screening of all human helicases reveals telomere-associated helicases modulate DPR expression

The regulatory mechanisms of RAN translation are not completely understood. However, previous studies provided evidence that the helicases DHX36 and DDX3X modulate DPR expression.[25,27,31] To determine if more helicases are involved, we performed an arrayed CRISPR-Cas9 knockout (CRISPRn)

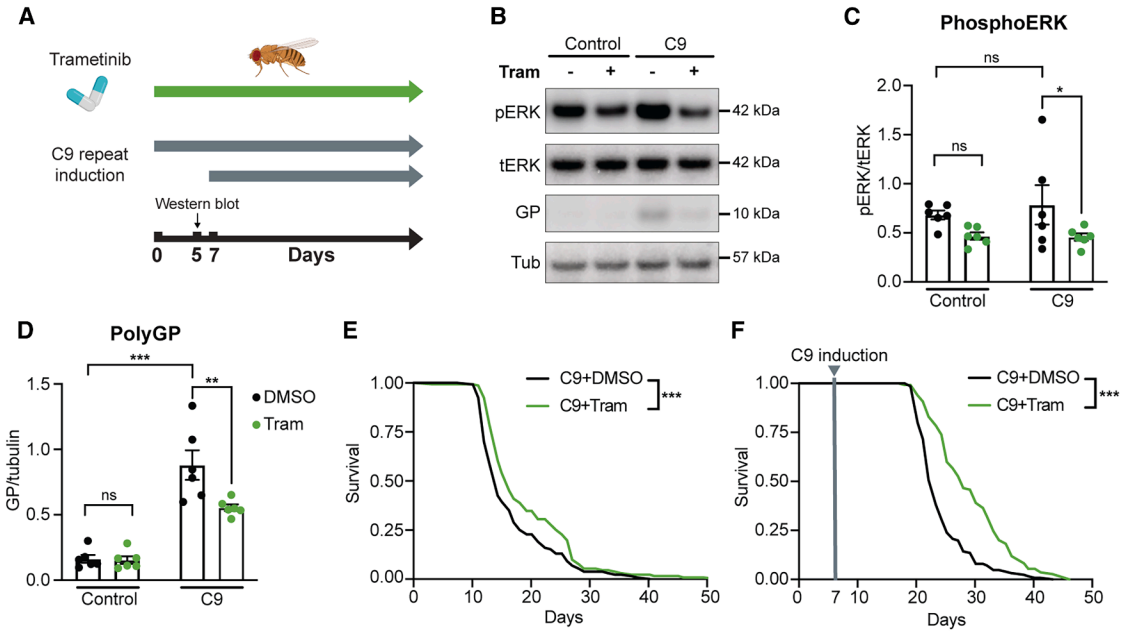

Figure 5. Trametinib reduces DPR levels and extends survival of *C9orf72* repeat expressing *Drosophila*

(A–D) (A) *Drosophila* experimental setup: after eclosion, flies were either fed trametinib (Tram) at 15.6 μM concurrently with the induction of the 36 GGGGCC (C9) repeat transgene, which is controlled by the inducible elavGS neuronal driver, or they were treated prophylactically with trametinib for 7 days before the induction of the C9 repeat transgene. Fly heads were collected for immunoblotting after 5 days of C9 repeat induction (with continual trametinib feeding). Control flies also harbor the C9 repeat transgene but are not induced. Western blot (B) and quantification showing the ratio of phosphorylated ERK (pERK) to total ERK (tERK) (C) and polyGP levels (D) after normalization with tubulin. Trametinib feeding significantly decreased pERK levels in the heads of C9 flies compared with DMSO-fed C9 flies (*p = 0.0409, uncorrected Fisher's LSD). Trametinib feeding also significantly decreased the levels of polyGP in C9 flies (**p = 0.0013, uncorrected Fisher's LSD). Bar charts show mean ± SEM, n = 6 biological replicates per condition with 10 heads per replicate.

(E) Survival curves showing trametinib significantly extends lifespan of C9 flies when drug treatment is initiated at the same time as C9 repeat induction (**p = 0.0016; log rank test; n = 150).

(F) Survival curves showing that pre-treatment with trametinib for 7 days before inducing C9 repeat expression significantly extends lifespan of C9 flies (***p = 1.57E−11, log rank test n = 150).

screen with a library comprising all 95 human helicases and 58 helicase-domain containing genes with redundant or no characterized function (153 genes in total). Experimental conditions were optimized using sgRNAs targeting *C9orf72*, achieving a knockout efficiency of 88.5% (Figures S13A–S13D). At 72 h post-neural induction, i^{3}N GA-HiBiT cells were nucleofected with 3 guide RNAs per gene and recombinant SpCas9 protein by 96-well nucleofection and then split into duplicate plates for imaging and luminescence/toxicity assays, respectively (Figure 6A). After 3 days of treatment, imaging plates were used to quantify the canonical translation reporter NLS-mApple as described (Figure S10G), with toxicity and luciferase assays performed on the duplicate plate. We performed the screen three times on independent inductions and determined cell viability and polyGA-HiBiT levels (Figure 6B). Hit genes were defined by reduction of polyGA-HiBiT levels 3×SD below the mean of control wells, without harboring toxicity. Previously reported RAN translation modifiers DDX3X and DHX36 did not fulfill hit gene criteria and did not affect polyGA-HiBiT levels using orthogonal knockdown or overexpression approaches (Figures S13E–S13M). However, we identified 15 hit genes that decrease polyGA-HiBiT levels upon knockout, with no genes identified that increase polyGA-HiBiT levels (Figure 6C). Five of the 15 genes, *ERCC8*, *RECQL*, *RECQL4, RTEL1*, and *UPF1* did not affect NLS-mApple levels, indicating enhanced specificity for RAN translation over canonical translation (Figure 7A). Moreover, knockdown of the aforementioned helicases did not affect sense/antisense RNA foci levels (Figures S14A–S14D) or *C9orf72* RNA expression levels (Figures S14E and S14F). Interestingly, DNA helicases (*RTEL1*, *RECQL*, *RECQL4*) were non-significantly enriched among screening hits compared with the entire library (60% of screen hits vs. 20% of the library are DNA helicases, p = 0.057) (Figure 7B).

To identify overlaps in regulatory function, we performed STRING analysis, combined with literature mining. We found that four of five helicase hits (80%, *RECQL*, *RECQL4, RTEL1*, and *UPF1*) are functionally involved in telomere homeostasis and maintenance, a significant enrichment compared with all human helicases (9.9%) (Figures 7C and 7D). Knockdown of each helicase and the consequent reduction in DPR levels were validated by western blotting (Figure 7E) and MSD immunoassay of polyGA (Figure 7F), respectively. Knockdown of each helicase also reduced polyGP levels in at least two of three independent, unedited patient-derived cell lines (Figure 7G). These data show that several telomere-associated helicases modulate the levels of endogenous DPRs, which confirms the ability of our platform

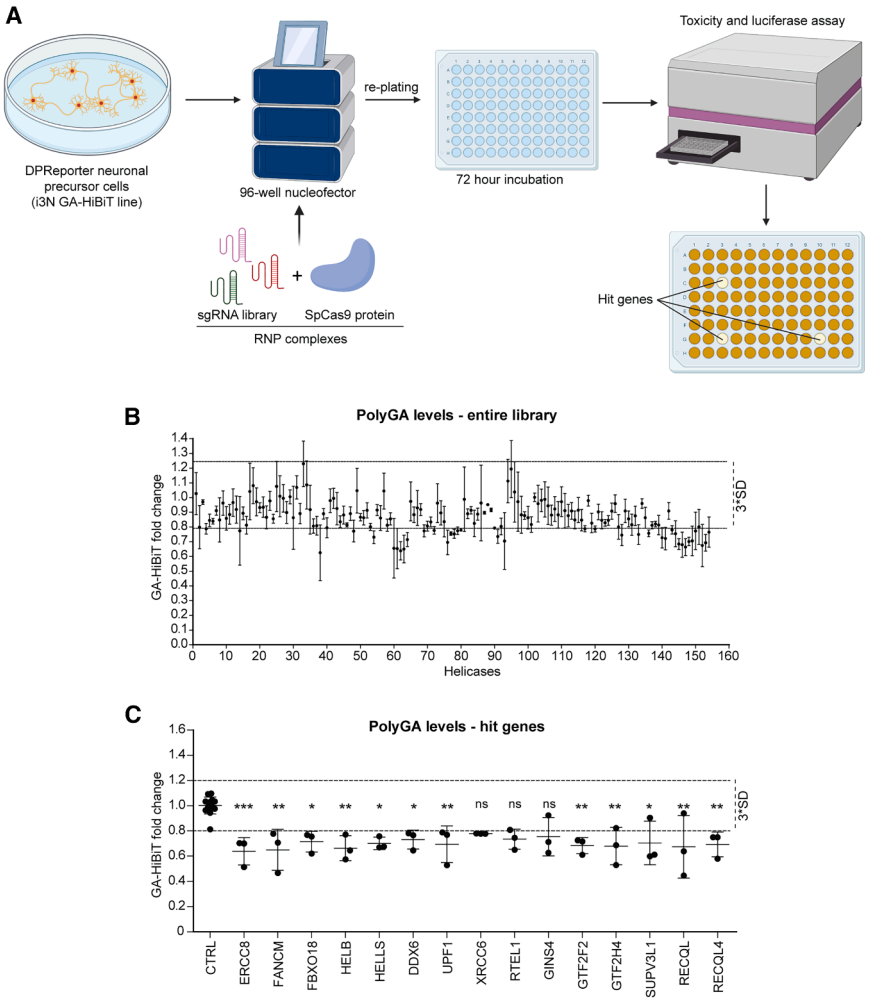

Figure 6. CRISPRn screening of a helicase library reveals modifiers of endogenous RAN translation

(A) Schematic representation of HTS workflow. DPReporter iPSCs are induced for 72 h before high-throughput nucleofection with helicase sgRNA library and recombinant Cas9 protein. Cells are cultured for 72 h before determining toxicity and polyGA-HiBiT levels.

(B) PolyGA-HiBiT levels after CRISPRn screening of the helicase library.

(C) Hit genes reducing polyGA-HiBiT levels in CRISPRn screen (*$p \leq 0.05$, **$p \leq 0.01$, ***$p \leq 0.001$, one-way ANOVA). Data are presented as mean ± SD, $N = 3$ independent screens, dotted lines = mean ± 3×SD window of control wells.

to enable arrayed, genetic CRISPR-based screening to identify modifiers of endogenous DPR expression.

DISCUSSION

We present a luciferase-based high-throughput screening method to investigate modulators of endogenous *C9orf72* DPR levels in iPSC-derived neurons. Large-scale approaches to fluorescently tag proteins have shown that low abundance proteins are not detectable with GFP or mNeonGreen.[47,48] Non-canonical RAN translation is unlikely to be as efficient as canonical translation and therefore endogenous RAN translated proteins, may be difficult to detect using a fluorescent tagging approach. Therefore, an important part of our strategy, which is readily applicable to studying endogenous RAN translated proteins in other repeat expansion disorders, is the use of the small and highly sensitive HiBiT tag, which allowed robust and rapid DPR detection without utilizing antibodies. We did not attempt to generate lines tagging endogenous polyGR because we have been unable to detect polyGR in *C9orf72* patient iPSC neurons using MSD immunoassay, and so focused on tagging polyGA and polyGP, which we felt had a higher chance of success. We performed extensive characterization of our lines and long-read sequencing showed that CRISPR-induced indels were more common at the 5′ end of the HiBiT insertion site. Several lines had small indels at this position, which is part of the intronic sequence downstream of the repeat expansion in *C9orf72* transcript variants 1 and 3 and part of non-coding exon 1b for *C9orf72* transcript variant 2. Despite this we did not observe changes in exon 1b usage, or clear effects on *C9orf72* transcript levels, and these lines still had utility for validation experiments, as they robustly generate DPRs, but we recommend using our i^{3}N GA-HiBiT line, which has a clean HiBiT insertion, as the primary line for screening. Placing long-read sequencing higher up in the cell line characterization workflow, now that it is becoming more readily available for repeat expansions, would also facilitate future development of repeat expansion reporter lines. Our long-read sequencing also showed that the sequence immediately downstream of the repeat is different for the unexpanded and expanded alleles, as previously reported,[49,50] which is important to note for future genetic targeting strategies.

A key feature of our platform is the use of the i^{3}Neuron system to provide rapid generation of neurons in large quantities within 5 days and the ability to multiplex with toxicity and live cell imaging assays to determine effects on cell viability, canonical translation, and potentially other imaging-based cellular phenotypes. This now provides a blueprint for studying endogenous RAN-translated proteins, at scale, in other repeat expansion disorders. We optimized and validated the platform for small-molecule screening in 384-well plate format and, utilizing a 1,444 natural product library, identified periplocin as an enhancer of DPR expression. Periplocin is a cardiac glycoside and notably, several other cardiac glycosides and steroid derivatives were found to be among the most potent DPR enhancers in our screen. These additional molecules were excluded due to their effects on global translation but may point to a relevant

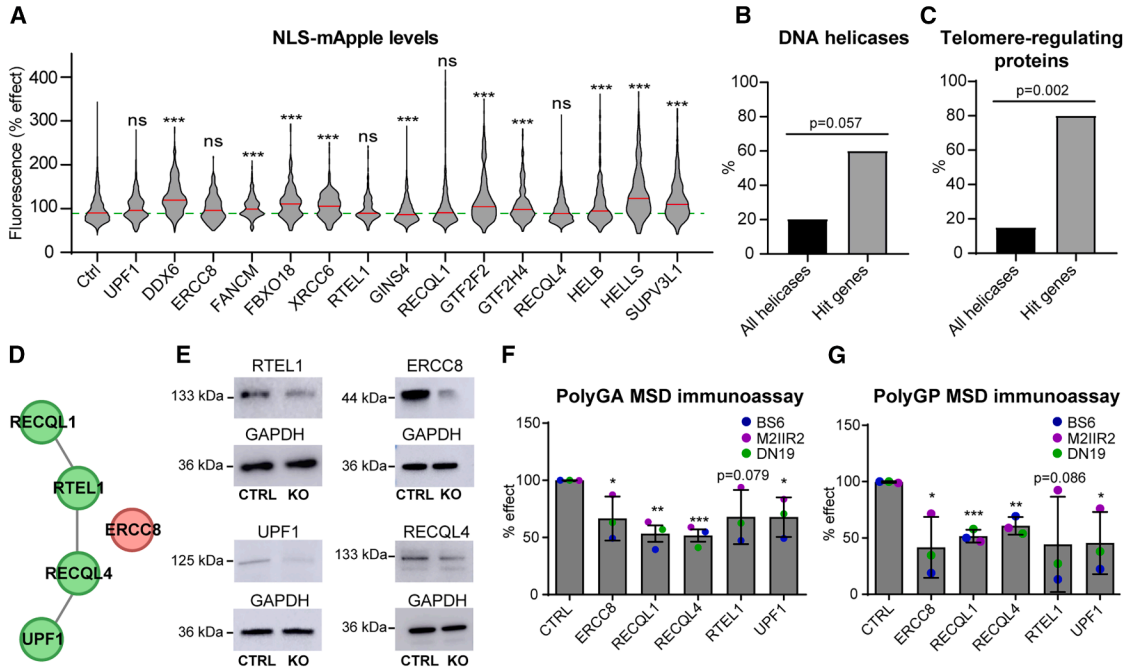

Figure 7. Telomere-associated helicases modulate DPR levels

(A) Quantification of canonical translation reporter NLS-mApple reveals effects of hit genes on global translation. Five of 15 hit genes (*UPF1*, *ERCC8*, *RTEL1*, *RECQL*, *RECQL4*) do not affect reporter expression (***$p \leq 0.001$, one-way ANOVA, red lines = median values, green line = DMSO median).

(B) DNA helicases are non-significantly enriched among screening hits (Fisher's exact test).

(C and D) Telomere-associated helicases are enriched among screening hits (80%) in comparison to all helicases (15%) (Fisher's exact test).

(E–G) Effect of knockdown of helicases on polyGA and polyGP levels in 3 independent *C9orf72* patient-derived iPSC lines (mean ± SD, *$p \leq 0.05$, **$p \leq 0.01$, ***$p \leq 0.001$, one-way ANOVA, $N = 3$ cell lines, median of 3 technical replicates per line).

structure-function relationship to investigate in the future. We found that periplocin treatment increased DPRs in a dose-dependent manner in our DPReporter lines and untagged patient lines. Periplocin inhibited the IRE1-XBP1 axis of the UPR, resulting in reduced XBP1 splicing, but knockdown of IRE1, which also reduced XBP1 splicing, did not increase DPRs. This indicated that the effect of periplocin on DPRs is not via XBP1. This was surprising as overexpression of XBP1 protects against *C9orf72* repeat toxicity in flies and mammalian ALS models,[51,52] but presumably via a general positive effect on proteostasis rather than modulating DPR levels.

Periplocin delayed the degradation of live-labeled endogenous DPRs and this effect correlated with ERK1/2 activation. Blocking ERK1/2 activation with the MEK1/2 inhibitor trametinib only partially abrogated periplocin's effect on DPRs, indicating that other mechanisms in addition to ERK1/2 activation may also contribute to periplocin's ability to increase DPRs. One possibility is an effect at the RNA level as periplocin also decreased the levels of both sense and antisense RNA foci. Reduction of RNA foci could lead to more soluble mRNA transcripts being available for transport out of the nucleus and subsequent RAN translation, but this will require further investigation to determine. However, strikingly, trametinib was able to reduce ERK1/2 activation, reduce DPRs, and extend lifespan in our well-established *C9orf72* repeat fly model.[17,53,54] The confirmation of this pathway in an *in vivo* model highlights the translatability of findings from our DPReporter lines, although it is important to note that the flies have considerably shorter repeats than the patient neurons, which could complicate a direct comparison. The mechanism of DPR reduction requires further experimentation, but one possibility is trametinib's reported enhancement of autophagy and lysosomal function.[55,56] Trametinib treatment was also shown to be beneficial to female SOD1 mice[57] and a trial in ALS is ongoing (ClinicalTrials.gov ID: NCT04326238). Further investigation is now warranted to determine if there is potential for repurposing MEK/ERK inhibitors specifically for C9FTD/ALS.

In addition, CRISPRn screening of 153 human helicases identified *ERCC8*, *RECQL*, *RECQL4*, *RTEL1*, and *UPF1* as enhancers of endogenous *C9orf72* RAN translation. Interestingly, UPF1 has previously been identified as a modulator of DPR levels, but in the opposite direction to our findings. Knockdown of UPF1 was shown to increase DPR levels and overexpression to reduce DPR levels in patient iPSC neurons.[58] The reasons for this are unclear but there is precedent for the same gene showing opposing effects on RAN translation in different studies, highlighting the complexity of the process.[29] That both studies independently identified UPF1 as a DPR modulator strengthens the case for its role in RAN translation. We did not observe an effect of two other helicases previously implicated in RAN translation, *DDX3X* and *DHX36*.[27,28,30,31] These differences between studies could be related to the use of different patient lines, different knockdown methods (siRNA, shRNA, CRISPR-Cas9), different

levels of knockdown, or the different differentiation protocols used (NGN2 overexpression to make cortical-like neurons vs. dual SMAD inhibition to generate spinal motor neurons). Encouragingly, decitabine, a nucleoside analog previously identified to reduce DPR levels through a primary screen in iPSC neurons,[35] was replicated in our DPReporter iPSC neurons. This provides confidence in decitabine as a genuine modifier and also shows that it is possible to find and replicate robust DPR modifiers in iPSC neurons.

Four of the five helicase hits are telomere-associated helicases.[59–62] By definition, these telomere-associated helicases are not specific for RAN translation, and it is unlikely that RAN translation-specific helicases exist. However, they suggest an overlap in the regulation of telomeres and the *C9orf72* repeat expansion. Human telomeres are TTAGGG hexanucleotide repeat sequences present at chromosomal ends that vary in size and can reach up to several kilobases.[63] Telomere shortening causes senescence, thus, their maintenance and elongation are tightly regulated.[64,65] They commonly form secondary structures such as T-loops and G-quadruplexes, which are bound by the telomere-machinery. In addition, similarly to the *C9orf72* repeat expansion, telomeres are transcribed into telomeric repeat-containing RNA (TERRA).[66] TERRAs regulate telomeric stability, length, and recruit chromatin-modifying enzymes.[67] Furthermore, a recent study revealed that TERRAs are translated into poly(valine-arginine) and poly(glycine-leucine) DPRs, which bind nucleic acids and are associated with replication forks, suggesting a regulatory function for telomere repeat-derived DPRs.[68] In summary, with their high G-content (50%) and tendency for secondary structure formation, telomeric repeats show similarities with *C9orf72* repeats. Given these similarities, there is a clear basis for *C9orf72* GGGGCC repeats to engage with helicases that also regulate telomeric repeats, but our helicase-wide screening approach was needed for this relationship to emerge. Outstanding questions are whether this interaction affects the normal regulation of telomeres, or whether telomere-associated helicases are affected by other repeat expansion disorders. Interestingly, recent evidence suggests that telomere length is misregulated in individuals with ALS.[69] Al Khleifat and colleagues report an increase in telomere length in both sporadic and familial ALS patients compared with controls. Telomere length in *C9orf72* ALS patients exceeded those of control individuals but was significantly shorter than in non-*C9orf72* ALS patients. These data suggest that telomere misregulation may be differently affected in *C9orf72* ALS patients. In addition, telomere length is shortened in other repeat expansion disorders, including HD and FXTAS[70,71]; however, the molecular mechanisms and relevance to disease pathogenesis are not known.

The DPR modulators we identified act similarly on both polyGA and polyGP. This was not necessarily expected as RAN translation of polyGA has been shown to be initiated by a near-cognate CUG start codon, whereas the nature of polyGP translation initiation is less clear.[21,22,24] As periplocin appears to reduce turnover of both polyGA and polyGP, this suggests a common mechanism can degrade both DPRs. While different mechanisms may be involved in the translation initiation of polyGA and polyGP, the helicases we identified most likely work upstream of translation by unwinding DNA to allow transcription of the repeat sequence, thus explaining the dual effect on both DPRs.

Limitations of the study

It is currently unclear whether the endogenous *C9orf72* GGGGCC repeat expansion is entirely pure, or whether the repeat expansion contains small interruptions. This raises a limitation of the study: in our lines designated as GA-HiBiT or GP-HiBiT, it is not possible to know whether HiBiT is tagging an entirely pure GA or GP repeat, or proteins that are a mixture of different DPRs. The long-read consensus sequence at the 3′ end of the repeat reading into the HiBiT tag shows a pure repeat in the expected frame for our reporter lines. However, each individual read shows interruptions in the repeat sequence, so it is not possible to know whether individual DPRs are pure or not. This is consistent with long-read sequencing of C9FTD/ALS patient cerebellar DNA, in which every read from a single individual showed different interruptions within the repeat.[2] All interruptions were motifs containing only Gs and Cs, so it is currently unclear whether these are genuine interruptions or sequencing errors. It is therefore possible that the HiBiT-tagged DPRs contain mixed DPRs, as these have been reported previously.[72] However, most important is that HiBiT is tagging the endogenous DPRs, so insights into modulation of endogenous DPRs can be gained, which was the key aim of the study. In addition, our lines do not allow immediate dissection of DPR vs. RNA toxicity, so we are unable to make an assessment of whether DPRs or repeat RNAs are the primary neurotoxic species in these lines.

All cell lines and protocols will be shared with the research community to facilitate understanding of *C9orf72* DPRs in ALS/FTD, and for the generation of additional high-throughput screening platforms for other repeat expansion disorders.

RESOURCE AVAILABILITY

Lead contact

Requests for materials and further information should be made to the lead contact, Adrian M. Isaacs (a.isaacs@ucl.ac.uk).

Materials availability

All cell lines generated in this publication will be shared upon request.

Data and code availability

- Data: long read DNA sequencing data are available at the Sequence Read Archive (SRA) accession no. PRJNA1236332.
- Code: custom scripts for analysis of long read sequencing of the *C9orf72* repeats are available at https://doi.org/10.5281/zenodo.14996789.
- Other items: any additional information required to reanalyze the data reported in this paper is available from the lead contact upon request.

ACKNOWLEDGMENTS

We thank Prof. Kevin Talbot (University of Oxford) for sharing a *C9orf72* patient-derived iPSC line. We are grateful to Jasmaine Lee at the UCL Long Read Sequencing Service for assistance with PacBio sequencing. We thank the Genomics England Scientific R&D team for sharing their protocol for genomic DNA preparation for the PromethION. This work was supported by Alzheimer's Research UK and the UK Dementia Research Institute

(UKDRI-1203) through UK DRI Ltd., principally funded by the Medical Research Council.

AUTHOR CONTRIBUTIONS

B.V.H., Y.G., P.M.M., K.M.W., L.M.G., P.F., S.J.T., and A.M.I. designed or supervised the experiments. B.T.S. and S.C. provided the parental cell line from which the DPReporters were generated. E.K. generated the i^{3}N C9 parental iPSC line. B.V.H. generated and characterized the DPReporter lines. A.M. performed bioinformatic analyses of exon usage. M.F., A.R.A., and C.L.F.-W. performed long-read sequencing. M.F. analyzed long-read sequencing data. N.O. performed Southern blotting with support from M.-D.R. and S.M. B.V.H. performed the small-molecule screen and CRISPRn screening. E.A. and P.W. contributed to the optimization of the small-molecule screening and provided the compound library and screening facilities. Y.G., P.M.M., H.K.D., B.V.H., D.V., L.K., and M.C. performed characterization of screening hits. M.L.A., E.U., R.A.G., A.G., and L.P. designed and performed *Drosophila* experiments. All authors discussed the data. B.V.H., Y.G., P.M.M., and A.M.I. wrote the paper with input from all authors.

DECLARATION OF INTERESTS

The authors declare no competing interests.

STAR★METHODS

Detailed methods are provided in the online version of this paper and include the following:

- KEY RESOURCES TABLE
- EXPERIMENTAL MODEL AND STUDY PARTICIPANT DETAILS
  - iPSC lines
  - Drosophila
- METHOD DETAILS
  - Culturing and passaging of iPSCs
  - Generation and induction of i^{3}Neurons
  - CRISPR/Cas9 tagging of *C9orf72* DPRs
  - MSD immunoassay
  - RNA-FISH for sense and antisense foci
  - Off-target sequencing and genetic integrity
  - Karyotyping
  - Long-read sequencing
  - PacBio sequencing
  - Nanopore adaptive long-read sequencing
  - DPR-HiBiT lytic detection assay
  - DPR-HiBiT live cell assay
  - DPR-HiBiT live labeling
  - Small molecule screening workflow
  - CRISPR screen workflow
  - Secondary screening workflow
  - Pathway analysis
  - RT-qPCR
  - Assay for quantification of exon1a/1b usage
  - Immunocytochemistry
  - Western blotting
  - Antisense oligonucleotide treatment of i^{3}Neurons
  - Cloning of lentiviral transfer plasmids
  - Lentiviral production and transduction
  - CRISPR-Cas9 mediated ERN1-knockdown
  - Southern blotting
- QUANTIFICATION AND STATISTICAL ANALYSIS

SUPPLEMENTAL INFORMATION

Supplemental information can be found online at https://doi.org/10.1016/j.celrep.2025.115695.

Received: June 21, 2023
Revised: November 4, 2024
Accepted: April 23, 2025
Published: May 10, 2025

REFERENCES

1. Renton, A.E., Majounie, E., Waite, A., Simón-Sánchez, J., Rollinson, S., Gibbs, J.R., Schymick, J.C., Laaksovirta, H., van Swieten, J.C., Myllykangas, L., et al. (2011). A Hexanucleotide Repeat Expansion in C9ORF72 Is the Cause of Chromosome 9p21-Linked ALS-FTD. Neuron *72*, 257–268. https://doi.org/10.1016/j.neuron.2011.09.010.
2. DeJesus-Hernandez, M., Mackenzie, I.R., Boeve, B.F., Boxer, A.L., Baker, M., Rutherford, N.J., Nicholson, A.M., Finch, N.A., Flynn, H., Adamson, J., et al. (2011). Expanded GGGGCC Hexanucleotide Repeat in Noncoding Region of C9ORF72 Causes Chromosome 9p-Linked FTD and ALS. Neuron *72*, 245–256. https://doi.org/10.1016/j.neuron.2011.09.011.
3. Todd, P.K., Oh, S., Krans, A., He, F., Sellier, C., Frazer, M., Renoux, A.J., Chen, K.c., Scaglione, K., Basrur, V., et al. (2013). CGG Repeat-Associated Translation Mediates Neurodegeneration in Fragile X Tremor Ataxia Syndrome. Neuron *78*, 440–455. https://doi.org/10.1016/j.neuron.2013.03.026.
4. Zu, T., Gibbens, B., Doty, N.S., Gomes-Pereira, M., Huguet, A., Stone, M.D., Margolis, J., Peterson, M., Markowski, T.W., Ingram, M.A.C., et al. (2011). Non-ATG-initiated translation directed by microsatellite expansions. Proc. Natl. Acad. Sci. USA *108*, 260–265. https://doi.org/10.1073/PNAS.1013343108.
5. Zu, T., Cleary, J.D., Liu, Y., Bañez-Coronel, M., Bubenik, J.L., Ayhan, F., Ashizawa, T., Xia, G., Clark, H.B., Yachnis, A.T., et al. (2017). RAN Translation Regulated by Muscleblind Proteins in Myotonic Dystrophy Type 2. Neuron *95*, 1292–1305.e5. https://doi.org/10.1016/J.NEURON.2017.08.039.
6. Bañez-Coronel, M., Ayhan, F., Tarabochia, A., Zu, T., Perez, B., Tusi, S., Pletnikova, O., Borchelt, D., Ross, C., Margolis, R., et al. (2015). RAN Translation in Huntington Disease. Neuron *88*, 667–677. https://doi.org/10.1016/j.neuron.2015.10.038.
7. Sznajder, Ł.J., and Swanson, M.S. (2019). Short Tandem Repeat Expansions and RNA-Mediated Pathogenesis in Myotonic Dystrophy. Int. J. Mol. Sci. *20*, 3365. https://doi.org/10.3390/IJMS20133365.
8. Ash, P.E.A., Bieniek, K.F., Gendron, T.F., Caulfield, T., Lin, W.-L., DeJesus-Hernandez, M., van Blitterswijk, M.M., Jansen-West, K., Paul, J.W., Rademakers, R., et al. (2013). Unconventional Translation of C9ORF72 GGGGCC Expansion Generates Insoluble Polypeptides Specific to c9FTD/ALS. Neuron *77*, 639–646. https://doi.org/10.1016/j.neuron.2013.02.004.
9. Gendron, T.F., Bieniek, K.F., Zhang, Y.J., Jansen-West, K., Ash, P.E.A., Caulfield, T., Daughrity, L., Dunmore, J.H., Castanedes-Casey, M., Chew, J., et al. (2013). Antisense transcripts of the expanded C9ORF72 hexanucleotide repeat form nuclear RNA foci and undergo repeat-associated non-ATG translation in c9FTD/ALS. Acta Neuropathol. *126*, 829–844. https://doi.org/10.1007/S00401-013-1192-8.
10. MacKenzie, I.R., Arzberger, T., Kremmer, E., Troost, D., Lorenzl, S., Mori, K., Weng, S.M., Haass, C., Kretzschmar, H.A., Edbauer, D., and Neumann, M. (2013). Dipeptide repeat protein pathology in C9ORF72 mutation cases: Clinico-pathological correlations. Acta Neuropathol. *126*, 859–879. https://doi.org/10.1007/s00401-013-1181-y.
11. Mori, K., Lammich, S., Mackenzie, I.R.A., Forné, I., Zilow, S., Kretzschmar, H., Edbauer, D., Janssens, J., Kleinberger, G., Cruts, M., et al. (2013). hnRNP A3 binds to GGGGCC repeats and is a constituent of p62-positive/TDP43-negative inclusions in the hippocampus of patients with C9orf72 mutations. Acta Neuropathol. *125*, 413–423. https://doi.org/10.1007/S00401-013-1088-7.
12. Mori, K., Weng, S.M., Arzberger, T., May, S., Rentzsch, K., Kremmer, E., Schmid, B., Kretzschmar, H.A., Cruts, M., Van Broeckhoven, C., et al.

(2013). The C9orf72 GGGGCC repeat is translated into aggregating dipeptide-repeat proteins in FTLD/ALS. Science *339*, 1335–1338. https://doi.org/10.1126/science.1232927.

13. Zu, T., Liu, Y., Bañez-Coronel, M., Reid, T., Pletnikova, O., Lewis, J., Miller, T.M., Harms, M.B., Falchook, A.E., Subramony, S.H., et al. (2013). RAN proteins and RNA foci from antisense transcripts in C9ORF72 ALS and frontotemporal dementia. Proc. Natl. Acad. Sci. USA *110*, E4968–E4977. https://doi.org/10.1073/pnas.1315438110.
14. Freibaum, B.D., Lu, Y., Lopez-Gonzalez, R., Kim, N.C., Almeida, S., Lee, K. H., Badders, N., Valentine, M., Miller, B.L., Wong, P.C., et al. (2015). GGGGCC repeat expansion in C9orf72 compromises nucleocytoplasmic transport. Nature *525*, 129–133. https://doi.org/10.1038/nature14974.
15. Lee, K.H., Zhang, P., Kim, H.J., Mitrea, D.M., Sarkar, M., Freibaum, B.D., Cika, J., Coughlin, M., Messing, J., Molliex, A., et al. (2016). C9orf72 Dipeptide Repeats Impair the Assembly, Dynamics, and Function of Membrane-Less Organelles. Cell *167*, 774–788.e17. https://doi.org/10.1016/J.CELL.2016.10.002.
16. Wen, X., Tan, W., Westergard, T., Krishnamurthy, K., Markandaiah, S.S., Shi, Y., Lin, S., Shneider, N.A., Monaghan, J., Pandey, U.B., et al. (2014). Antisense Proline-Arginine RAN dipeptides linked to C9ORF72-ALS/FTD form toxic nuclear aggregates that initiate in vitro and in vivo neuronal death. Neuron *84*, 1213–1225. https://doi.org/10.1016/J.NEURON.2014.12.010.
17. Mizielinska, S., Grönke, S., Niccoli, T., Ridler, C.E., Clayton, E.L., Devoy, A., Moens, T., Norona, F.E., Woollacott, I.O.C., Pietrzyk, J., et al. (2014). C9orf72 repeat expansions cause neurodegeneration in Drosophila through arginine-rich proteins. Science *345*, 1192–1194. https://doi.org/10.1126/science.1256800.
18. Gendron, T.F., and Petrucelli, L. (2018). Disease Mechanisms of C9ORF72 Repeat Expansions. Cold Spring Harb. Perspect. Med. *8*, a024224. https://doi.org/10.1101/CSHPERSPECT.A024224.
19. Moens, T.G., Partridge, L., and Isaacs, A.M. (2017). Genetic models of C9orf72: what is toxic? Curr. Opin. Genet. Dev. *44*, 92–101.
20. Almeida, S., Krishnan, G., Rushe, M., Gu, Y., Kankel, M.W., and Gao, F.-B. (2019). Production of poly(GA) in C9ORF72 patient motor neurons derived from induced pluripotent stem cells. Acta Neuropathol. *138*, 1099–1101. https://doi.org/10.1007/s00401-019-02083-z.
21. Cheng, W., Wang, S., Mestre, A.A., Fu, C., Makarem, A., Xian, F., Hayes, L. R., Lopez-Gonzalez, R., Drenner, K., Jiang, J., et al. (2018). C9ORF72 GGGGCC repeat-associated non-AUG translation is upregulated by stress through eIF2α phosphorylation. Nat. Commun. *9*, 51. https://doi.org/10.1038/s41467-017-02495-z.
22. Green, K.M., Glineburg, M.R., Kearse, M.G., Flores, B.N., Linsalata, A.E., Fedak, S.J., Goldstrohm, A.C., Barmada, S.J., and Todd, P.K. (2017). RAN translation at C9orf72-associated repeat expansions is selectively enhanced by the integrated stress response. Nat. Commun. *8*, 2005. https://doi.org/10.1038/s41467-017-02200-0.
23. Sonobe, Y., Lee, S., Krishnan, G., Gu, Y., Kwon, D.Y., Gao, F.-B., Roos, R. P., and Kratsios, P. (2023). Translation of dipeptide repeat proteins in C9ORF72-ALS/FTD through unique and redundant AUG initiation codons. Elife *12*, e83189. https://doi.org/10.7554/eLife.83189.
24. Tabet, R., Schaeffer, L., Freyermuth, F., Jambeau, M., Workman, M., Lee, C.-Z., Lin, C.-C., Jiang, J., Jansen-West, K., Abou-Hamdan, H., et al. (2018). CUG initiation and frameshifting enable production of dipeptide repeat proteins from ALS/FTD C9ORF72 transcripts. Nat. Commun. *9*, 152. https://doi.org/10.1038/s41467-017-02643-5.
25. Liu, H., Lu, Y.N., Paul, T., Periz, G., Banco, M.T., Ferré-D'Amaré, A.R., Rothstein, J.D., Hayes, L.R., Myong, S., and Wang, J. (2021). A Helicase Unwinds Hexanucleotide Repeat RNA G-Quadruplexes and Facilitates Repeat-Associated Non-AUG Translation. J. Am. Chem. Soc. *143*, 7368–7379. https://doi.org/10.1021/JACS.1C00131.
26. Yamada, S.B., Gendron, T.F., Niccoli, T., Genuth, N.R., Grosely, R., Shi, Y., Glaria, I., Kramer, N.J., Nakayama, L., Fang, S., et al. (2019). RPS25 is required for efficient RAN translation of C9orf72 and other neurodegenerative disease-associated nucleotide repeats. Nat. Neurosci. *22*, 1383–1388. https://doi.org/10.1038/s41593-019-0455-7.
27. Tseng, Y.J., Sandwith, S.N., Green, K.M., Chambers, A.E., Krans, A., Raimer, H.M., Sharlow, M.E., Reisinger, M.A., Richardson, A.E., Routh, E.D., et al. (2021). The RNA helicase DHX36–G4R1 modulates C9orf72 GGGGCC hexanucleotide repeat–associated translation. J. Biol. Chem. *297*, 100914. https://doi.org/10.1016/J.JBC.2021.100914.
28. Linsalata, A.E., He, F., Malik, A.M., Glineburg, M.R., Green, K.M., Natla, S., Flores, B.N., Krans, A., Archbold, H.C., Fedak, S.J., et al. (2019). DDX 3X and specific initiation factors modulate *FMR 1* repeat-associated non-AUG-initiated translation. EMBO Rep. *20*, e47498. https://doi.org/10.15252/embr.201847498.
29. Wilson, K.M., Muralidharan, B., and Isaacs, A.M. (2019). Relax, Don't RAN Translate It. Neuron *104*, 827–829. https://doi.org/10.1016/j.neuron.2019.11.014.
30. Fu, X., Zhang, Z., Hayes, L.R., Wright, N., Asbury, J., Li, S., Ye, Y., and Sun, S. (2024). DDX3X overexpression decreases dipeptide repeat proteins in a mouse model of C9ORF72-ALS/FTD. Exp. Neurol. *376*, 114768. https://doi.org/10.1016/J.EXPNEUROL.2024.114768.
31. Cheng, W., Wang, S., Zhang, Z., Morgens, D.W., Hayes, L.R., Lee, S., Portz, B., Xie, Y., Nguyen, B.V., Haney, M.S., et al. (2019). CRISPR-Cas9 Screens Identify the RNA Helicase DDX3X as a Repressor of C9ORF72 (GGGGCC)n Repeat-Associated Non-AUG Translation. Neuron *104*, 885–898.e8. https://doi.org/10.1016/J.NEURON.2019.09.003.
32. Gendron, T.F., Chew, J., Stankowski, J.N., Hayes, L.R., Zhang, Y.J., Prudencio, M., Carlomagno, Y., Daughrity, L.M., Jansen-West, K., Perkerson, E.A., et al. (2017). Poly(GP) proteins are a useful pharmacodynamic marker for C9ORF72-associated amyotrophic lateral sclerosis. Sci. Transl. Med. *9*, eaai7866. https://doi.org/10.1126/SCITRANSLMED.AAI7866.
33. Quaegebeur, A., Glaria, I., Lashley, T., and Isaacs, A.M. (2020). Soluble and insoluble dipeptide repeat protein measurements in C9orf72-frontotemporal dementia brains show regional differential solubility and correlation of poly-GR with clinical severity. Acta Neuropathol. Commun. *8*, 184. https://doi.org/10.1186/S40478-020-01036-Y/TABLES/4.
34. Wilson, K.M., Katona, E., Glaria, I., Carcolé, M., Swift, I.J., Sogorb-Esteve, A., Heller, C., Bouzigues, A., Heslegrave, A.J., Keshavan, A., et al. (2022). Development of a sensitive trial-ready poly(GP) CSF biomarker assay for *C9orf72*-associated frontotemporal dementia and amyotrophic lateral sclerosis. J. Neurol. Neurosurg. Psychiatry *93*, 761–771. https://doi.org/10.1136/JNNP-2021-328710.
35. Czuppa, M., Dhingra, A., Zhou, Q., Schludi, C., König, L., Scharf, E., Farny, D., Dalmia, A., Täger, J., Castillo-Lizardo, M., et al. (2022). Drug screen in iPSC-Neurons identifies nucleoside analogs as inhibitors of (G4C2)n expression in C9orf72 ALS/FTD. Cell Rep. *39*, 110913. https://doi.org/10.1016/J.CELREP.2022.110913.
36. Wang, C., Ward, M.E., Chen, R., Liu, K., Tracy, T.E., Chen, X., Xie, M., Sohn, P.D., Ludwig, C., Meyer-Franke, A., et al. (2017). Scalable Production of iPSC-Derived Human Neurons to Identify Tau-Lowering Compounds by High-Content Screening. Stem Cell Rep. *9*, 1221–1233. https://doi.org/10.1016/J.STEMCR.2017.08.019.
37. Fernandopulle, M.S., Prestil, R., Grunseich, C., Wang, C., Gan, L., and Ward, M.E. (2018). Transcription Factor-Mediated Differentiation of Human iPSCs into Neurons. Curr. Protoc. Cell Biol. *79*, e51. https://doi.org/10.1002/cpcb.51.
38. Licata, N.V., Cristofani, R., Salomonsson, S., Wilson, K.M., Kempthorne, L., Vaizoglu, D., D'Agostino, V.G., Pollini, D., Loffredo, R., Pancher, M., et al. (2022). C9orf72 ALS/FTD dipeptide repeat protein levels are reduced by small molecules that inhibit PKA or enhance protein degradation. EMBO J. *41*, e105026. https://doi.org/10.15252/EMBJ.2020105026.
39. Simone, R., Balendra, R., Moens, T.G., Preza, E., Wilson, K.M., Heslegrave, A., Woodling, N.S., Niccoli, T., Gilbert-Jaramillo, J., Abdelkarim, S., et al. (2018). G-quadruplex-binding small molecules ameliorate C9orf72 FTD/ALS pathology in vitro and in vivo. EMBO Mol. Med. *10*, 22–31. https://doi.org/10.15252/EMMM.201707850.

40. Lagier-Tourenne, C., Baughn, M., Rigo, F., Sun, S., Liu, P., Li, H.R., Jiang, J., Watt, A.T., Chun, S., Katz, M., et al. (2013). Targeted degradation of sense and antisense C9orf72 RNA foci as therapy for ALS and frontotemporal degeneration. Proc. Natl. Acad. Sci. USA *110*, E4530–E4539. https://doi.org/10.1073/pnas.1318835110.

41. Jasial, S., Hu, Y., and Bajorath, J. (2017). How Frequently Are Pan-Assay Interference Compounds Active? Large-Scale Analysis of Screening Data Reveals Diverse Activity Profiles, Low Global Hit Frequency, and Many Consistently Inactive Compounds. J. Med. Chem. *60*, 3879–3886. https://doi.org/10.1021/ACS.JMEDCHEM.7B00154/ASSET/IMAGES/LARGE/JM-2017-00154Z_0004.JPEG.

42. Tokugawa, M., Inoue, Y., Ishiuchi, K., Kujirai, C., Matsuno, M., Ri, M., Itoh, Y., Miyajima, C., Morishita, D., Ohoka, N., et al. (2021). Periplocin and cardiac glycosides suppress the unfolded protein response. Sci. Rep. *11*, 9528. https://doi.org/10.1038/s41598-021-89074-x.

43. Lu, Z.J., Zhou, Y., Song, Q., Qin, Z., Zhang, H., Zhou, Y.J., Gou, L.T., Yang, J.L., and Luo, F. (2010). Periplocin inhibits growth of lung cancer in vitro and in vivo by blocking AKT/ERK signaling pathways. Cell. Physiol. Biochem. *26*, 609–618. https://doi.org/10.1159/000322328.

44. Read, A., and Schröder, M. (2021). The Unfolded Protein Response: An Overview. Biology *10*, 384. https://doi.org/10.3390/BIOLOGY10050384.

45. Gallagher, C.M., Garri, C., Cain, E.L., Ang, K.K.H., Wilson, C.G., Chen, S., Hearn, B.R., Jaishankar, P., Aranda-Diaz, A., Arkin, M.R., et al. (2016). Ceapins are a new class of unfolded protein response inhibitors, selectively targeting the ATF6α branch. Elife *5*, e11878. https://doi.org/10.7554/ELIFE.11878.

46. Roskoski, R. (2019). Targeting ERK1/2 protein-serine/threonine kinases in human cancers. Pharmacol. Res. *142*, 151–168. https://doi.org/10.1016/J.PHRS.2019.01.039.

47. Cho, N.H., Cheveralls, K.C., Brunner, A.D., Kim, K., Michaelis, A.C., Raghavan, P., Kobayashi, H., Savy, L., Li, J.Y., Canaj, H., et al. (2022). OpenCell: Endogenous tagging for the cartography of human cellular organization. Science *375*, eabi6983. https://doi.org/10.1126/SCIENCE.ABI6983.

48. Leonetti, M.D., Sekine, S., Kamiyama, D., Weissman, J.S., and Huang, B. (2016). A scalable strategy for high-throughput GFP tagging of endogenous human proteins. Proc. Natl. Acad. Sci. USA *113*, E3501–E3508. https://doi.org/10.1073/PNAS.1606731113.

49. van der Zee, J., Gijselinck, I., Dillen, L., Van Langenhove, T., Theuns, J., Engelborghs, S., Philtjens, S., Vandenbulcke, M., Sleegers, K., Sieben, A., et al. (2013). A Pan-European Study of the C9orf72 Repeat Associated with FTLD: Geographic Prevalence, Genomic Instability, and Intermediate Repeats. Hum. Mutat. *34*, 363–373. https://doi.org/10.1002/HUMU.22244.

50. Nair, R.R., Tibbit, C., Thompson, D., McLeod, R., Nakhuda, A., Simon, M. M., Baloh, R.H., Fisher, E.M.C., Isaacs, A.M., and Cunningham, T.J. (2021). Sizing, stabilising, and cloning repeat-expansions for gene targeting constructs. Methods *191*, 15–22. https://doi.org/10.1016/J.YMETH.2020.07.007.

51. Shen, D., Vincent, A., Udine, E., Buhidma, Y., Anoar, S., Tsintzas, E., Maeland, M., Rademakers, R., Isaacs, A.M., Frigerio, C., et al. (2023). Differential neuronal vulnerability to C9orf72 repeat expansion driven by Xbp1 transcription signature. Preprint at bioRxiv. https://doi.org/10.1101/2023.11.20.567861.

52. Valenzuela, V., Becerra, D., Astorga, J.I., Fuentealba, M., Diaz, G., Bargsted, L., Chacón, C., Martinez, A., Gozalvo, R., Jackson, K., et al. (2025). Artificial enforcement of the unfolded protein response reduces disease features in multiple preclinical models of ALS/FTD. Mol. Ther. *33*, 1226–1245. https://doi.org/10.1016/j.ymthe.2025.01.004.

53. Atilano, M.L., Grönke, S., Niccoli, T., Kempthorne, L., Hahn, O., Morón-Oset, J., Hendrich, O., Dyson, M., Adams, M.L., Hull, A., et al. (2021). Enhanced insulin signalling ameliorates C9orf72 hexanucleotide repeat expansion toxicity in Drosophila. Elife *10*, e58565. https://doi.org/10.7554/ELIFE.58565.

54. Moens, T.G., Niccoli, T., Wilson, K.M., Atilano, M.L., Birsa, N., Gittings, L. M., Holbling, B.V., Dyson, M.C., Thoeng, A., Neeves, J., et al. (2019). C9orf72 arginine-rich dipeptide proteins interact with ribosomal proteins in vivo to induce a toxic translational arrest that is rescued by eIF1A. Acta Neuropathol. *137*, 487–500. https://doi.org/10.1007/s00401-018-1946-4.

55. Kinsey, C.G., Camolotto, S.A., Boespflug, A.M., Guillen, K.P., Foth, M., Truong, A., Schuman, S.S., Shea, J.E., Seipp, M.T., Yap, J.T., et al. (2019). Protective autophagy elicited by RAF→MEK→ERK inhibition suggests a treatment strategy for RAS-driven cancers. Nat. Med. *25*, 620–627. https://doi.org/10.1038/S41591-019-0367-9.

56. Chun, Y.S., Kim, M.Y., Lee, S.Y., Kim, M.J., Hong, T.J., Jeon, J.K., Ganbat, D., Kim, H.T., Kim, S.S., Kam, T.I., and Han, S. (2022). MEK1/2 inhibition rescues neurodegeneration by TFEB-mediated activation of autophagic lysosomal function in a model of Alzheimer's Disease. Mol. Psychiatr. *27*, 4770–4780. https://doi.org/10.1038/S41380-022-01713-5.

57. Caldi Gomes, L., Hänzelmann, S., Hausmann, F., Khatri, R., Oller, S., Parvaz, M., Tzeplaeff, L., Pasetto, L., Gebelin, M., Ebbing, M., et al. (2024). Multiomic ALS signatures highlight subclusters and sex differences suggesting the MAPK pathway as therapeutic target. Nat. Commun. *15*, 1–23. https://doi.org/10.1038/s41467-024-49196-y.

58. Zaepfel, B.L., Zhang, Z., Maulding, K., Coyne, A.N., Cheng, W., Hayes, L. R., Lloyd, T.E., Sun, S., and Rothstein, J.D. (2021). UPF1 reduces C9orf72 HRE-induced neurotoxicity in the absence of nonsense-mediated decay dysfunction. Cell Rep. *34*, 108925. https://doi.org/10.1016/J.CELREP.2021.108925.

59. Chawla, R., Redon, S., Raftopoulou, C., Wischnewski, H., Gagos, S., and Azzalin, C.M. (2011). Human UPF1 interacts with TPP1 and telomerase and sustains telomere leading-strand replication. EMBO J. *30*, 4047–4058. https://doi.org/10.1038/EMBOJ.2011.280.

60. Deng, Z., Glousker, G., Molczan, A., Fox, A.J., Lamm, N., Dheekollu, J., Weizman, O.E., Schertzer, M., Wang, Z., Vladimirova, O., et al. (2013). Inherited mutations in the helicase RTEL1 cause telomere dysfunction and Hoyeraal-Hreidarsson syndrome. Proc. Natl. Acad. Sci. USA *110*, E3408. https://doi.org/10.1073/PNAS.1300600110/-/DCSUPPLEMENTAL.

61. Luong, T.T., and Bernstein, K.A. (2021). Role and Regulation of the RECQL4 Family during Genomic Integrity Maintenance. Genes *12*, 1919. https://doi.org/10.3390/GENES12121919.

62. Popuri, V., Hsu, J., Khadka, P., Horvath, K., Liu, Y., Croteau, D.L., and Bohr, V.A. (2014). Human RECQL1 participates in telomere maintenance. Nucleic Acids Res. *42*, 5671–5688. https://doi.org/10.1093/NAR/GKU200.

63. Harley, C.B., Futcher, A.B., and Greider, C.W. (1990). Telomeres shorten during ageing of human fibroblasts. Nature *345*, 458–460. https://doi.org/10.1038/345458a0.

64. Allsopp, R.C., Vaziri, H., Patterson, C., Goldstein, S., Younglai, E.V., Futcher, A.B., Greider, C.W., and Harley, C.B. (1992). Telomere length predicts replicative capacity of human fibroblasts. Proc. Natl. Acad. Sci. USA *89*, 10114–10118. https://doi.org/10.1073/PNAS.89.21.10114.

65. Rodier, F., Kim, S.H., Nijjar, T., Yaswen, P., and Campisi, J. (2005). Cancer and aging: the importance of telomeres in genome maintenance. Int J Biochem Cell Biol *37*, 977–990. https://doi.org/10.1016/j.biocel.2004.10.012.

66. Azzalin, C.M., Reichenbach, P., Khoriauli, L., Giulotto, E., and Lingner, J. (2007). Telomeric repeat containing RNA and RNA surveillance factors at mammalian chromosome ends. Science *318*, 798–801. https://doi.org/10.1126/SCIENCE.1147182.

67. Azzalin, C.M., and Lingner, J. (2015). Telomere functions grounding on TERRA firma. Trends Cell Biol. *25*, 29–36. https://doi.org/10.1016/J.TCB.2014.08.007.

68. Al-Turki, T.M., and Griffith, J.D. (2023). Mammalian telomeric RNA (TERRA) can be translated to produce valine-arginine and glycine-leucine dipeptide repeat proteins. Proc. Natl. Acad. Sci. USA *120*, e2221529120. https://doi.org/10.1073/PNAS.2221529120.

69. Al Khleifat, A., Iacoangeli, A., Jones, A.R., van Vugt, J.J.F.A., Moisse, M., Shatunov, A., Zwamborn, R.A.J., van der Spek, R.A.A., Cooper-Knock, J., Topp, S., et al. (2022). Telomere length analysis in amyotrophic lateral sclerosis using large-scale whole genome sequence data. Front. Cell. Neurosci. *16*, 1050596. https://doi.org/10.3389/FNCEL.2022.1050596.

70. Jenkins, E.C., Tassone, F., Ye, L., Gu, H., Xi, M., Velinov, M., Brown, W.T., Hagerman, R.J., and Hagerman, P.J. (2008). Reduced Telomere Length in older Men with Premutation Alleles of the Fragile X Mental Retardation 1 Gene. Am. J. Med. Genet. *146A*, 1543–1546. https://doi.org/10.1002/AJMG.A.32342.

71. Scarabino, D., Veneziano, L., Peconi, M., Frontali, M., Mantuano, E., and Corbo, R.M. (2019). Leukocyte telomere shortening in Huntington's disease. J. Neurol. Sci. *396*, 25–29. https://doi.org/10.1016/J.JNS.2018.10.024.

72. McEachin, Z.T., Gendron, T.F., Raj, N., García-Murias, M., Banerjee, A., Purcell, R.H., Ward, P.J., Todd, T.W., Merritt-Garza, M.E., Jansen-West, K., et al. (2020). Chimeric Peptide Species Contribute to Divergent Dipeptide Repeat Pathology in c9ALS/FTD and SCA36. Neuron *107*, 292–305.e6. https://doi.org/10.1016/j.neuron.2020.04.011.

73. Ababneh, N.A., Scaber, J., Flynn, R., Douglas, A., Barbagallo, P., Candalija, A., Turner, M.R., Sims, D., Dafinca, R., Cowley, S.A., and Talbot, K. (2020). Correction of amyotrophic lateral sclerosis related phenotypes in induced pluripotent stem cell-derived motor neurons carrying a hexanucleotide expansion mutation in C9orf72 by CRISPR/Cas9 genome editing using homology-directed repair. Hum. Mol. Genet. *29*, 2200–2217. https://doi.org/10.1093/HMG/DDAA106.

74. Selvaraj, B.T., Livesey, M.R., Zhao, C., Gregory, J.M., James, O.T., Cleary, E.M., Chouhan, A.K., Gane, A.B., Perkins, E.M., Dando, O., et al. (2018). C9ORF72 repeat expansion causes vulnerability of motor neurons to Ca2+-permeable AMPA receptor-mediated excitotoxicity. Nat. Commun. *9*, 347. https://doi.org/10.1038/s41467-017-02729-0.

75. Pliatsika, V., and Rigoutsos, I. (2015). "Off-Spotter": very fast and exhaustive enumeration of genomic lookalikes for designing CRISPR/Cas guide RNAs. Biol. Direct *10*, 4. https://doi.org/10.1186/s13062-015-0035-z.

76. Berg, S., Kutra, D., Kroeger, T., Straehle, C.N., Kausler, B.X., Haubold, C., Schiegg, M., Ales, J., Beier, T., Rudy, M., et al. (2019). ilastik: interactive machine learning for (bio)image analysis. Nat. Methods *16*, 1226–1232. https://doi.org/10.1038/s41592-019-0582-9.

77. Li, H. (2018). Minimap2: pairwise alignment for nucleotide sequences. Bioinformatics *34*, 3094–3100. https://doi.org/10.1093/BIOINFORMATICS/BTY191.

78. Quinlan, A.R., and Hall, I.M. (2010). BEDTools: a flexible suite of utilities for comparing genomic features. Bioinformatics *26*, 841–842. https://doi.org/10.1093/BIOINFORMATICS/BTQ033.

STAR★METHODS

KEY RESOURCES TABLE

REAGENT or RESOURCE	SOURCE	IDENTIFIER
Antibodies		
Donkey polyclonal anti-rabbit IgG Alexa Fluor 488	BioLegend	Cat# 406416, RRID:AB_2563203
Goat DyLight 488 anti-Digoxigenin/Digoxin	Vector Laboratories	Cat# DI-7488, RRID:AB_2336399
Goat polyclonal anti-mouse IgG2a Alexa Fluor 488	Thermo Fisher Scientific	Cat# A-21131, RRID:AB_2535771
Goat polyclonal anti-mouse IgG H&L (HRP)	Abcam	Cat# ab6789, RRID:AB_955439
Goat polyclonal anti-rabbit IgG Alexa Fluor 546	Thermo Fisher Scientific	Cat# A-11035, RRID:AB_2534093
Goat polyclonal anti-Rabbit IgG H&L (HRP)	Abcam	Cat# ab6721, RRID:AB_955447
Mouse monoclonal anti-alpha tubulin	Sigma-Aldrich	Cat# T6199, RRID:AB_477583
Mouse monoclonal anti-C9orf72 [GT1553]	GeneTex	Cat# GTX634482, RRID:AB_2784545
Mouse monoclonal anti-C9ORF72/C9RANT (anti-poly-GA)	Millipore	Cat# MABN889, RRID:AB_2728663
Mouse monoclonal anti-GluR2 (6C4)	Thermo Fisher Scientific	Cat# 32–0300, RRID:AB_2533058
Mouse monoclonal anti-Map2, clone AP20	Millipore	Cat# MAB3418, RRID:AB_94856
Mouse monoclonal anti-poly-GA (GA5F2)	Dieter Edbauer	N/A
Mouse monoclonal anti-UPF1	Proteintech	Cat# 66898-1-Ig, RRID:AB_2882227
Rabbit monoclonal anti-eIF2α (D7D3) XP®	Cell Signaling Technology	Cat# 62928
Rabbit monoclonal anti-ERCC8 [EPR9237]	Abcam	Cat# ab137033, RRID:AB_2783825
Rabbit monoclonal anti-Erk1/2	Cell Signaling Technology	Cat# 4695; RRID:AB_390779
Rabbit monoclonal anti-GAPDH (Clone 14C10)	Cell Signaling Technology	Cat# 2118, RRID:AB_561053
Rabbit monoclonal anti-phospho Erk1/2	Cell Signaling Technology	Cat# 4370; RRID:AB_2315112
Rabbit monoclonal anti-Phospho-eIF2alpha (Ser51) (D9G8)	Cell Signaling Technology	Cat# 3398, RRID:AB_2096481
Rabbit monoclonal anti-PKR, phospho (Thr446), Clone E120	Abcam	Cat# ab32036, RRID:AB_777310
Rabbit monoclonal anti-RECQL1 [EPR8048]	Abcam	Cat# ab150421, RRID:AB_2892783
Rabbit monoclonal anti-Sox2	Cell Signaling Technology	Cat# 3579, RRID:AB_2195767
Rabbit monoclonal anti-XBP-1s (D2C1F)	Cell Signaling Technology	Cat# 12782, RRID:AB_2687943
Rabbit monoclonal anti-β3-Tubulin (D71G9) TUJ1	Cell Signaling Technology	Cat# 5568, RRID:AB_10694505
Rabbit monoclonal PKR antibody [Y117]	Abcam	Cat# ab32506, RRID:AB_777306
Rabbit polyclonal anti-AMPK alpha-1,2	Thermo Fisher Scientific	Cat# PA5-36045, RRID:AB_2553341
Rabbit polyclonal anti-GABAA Receptor (alpha1 subunit)	Sigma-Aldrich	Cat# G4416, RRID:AB_477016
Rabbit polyclonal anti-GP (GP658)	Eurogentec	Custom made
Rabbit polyclonal anti-Oct4	Cell Signaling Technology	Cat# 2750, RRID:AB_823583
Rabbit polyclonal anti-RECQL4	Abcam	Cat# ab188125
Rabbit polyclonal anti-RTEL1	Proteintech	Cat# 25337-1-AP, RRID:AB_2880034
Chemicals, peptides, and recombinant proteins		
ACCUTASE™	STEMCELL Technologies	Cat# 07922
Clontech Labs 3P Lenti-X™ Concentrator, 500 mL	Clontech Labs 3P	Cat# 631232
CSPD ready-to-use	Sigma-Aldrich	Cat# 11755633001
Denatured salmon sperm	ThermoFisher	Cat# 15632011
DIG Wash and Block Buffer Set	Roche	Cat# 11585762001
DIG-labelled DNA molecular weight marker VII	Sigma-Aldrich	Cat# 11669940910
DMSO	Sigma-Aldrich	Cat# D2650
DreamTaq PCR Master Mixes (2X)	ThermoFisher Scientific	Cat# K1071
Hoechst Stain solution	Sigma-Aldrich	Cat# H6024
DMEM:F12	Gibco (Thermo)	Cat# 10565018
N2 Supplement	Gibco (Thermo)	Cat# 17502048

(*Continued on next page*)

Continued

REAGENT or RESOURCE	SOURCE	IDENTIFIER
Non-essential amino acids	Gibco (Thermo)	Cat# 11140050
HEPES	Gibco (Thermo)	Cat# 15630056
Glutamax	Gibco (Thermo)	Cat# 35050061
Doxycycline Hyclate	Sigma/Merck	Cat# D9891
Rock inhibitor Y-27632	Miltenyi	Cat# 130-103-922
Neurobasal	Gibco (Thermo)	Cat# 12348017
B27 Supplement	Gibco (Thermo)	Cat# 17504044
BDNF	Gibco (Thermo)	Cat# 10908-010
NT-3	Peprotech	Cat# 450-03
Laminin	Merck Life Science	Cat# L2020-1MG
Lipofectamine™ 3000 Transfection Reagent	ThermoFisher Scientific	Cat# L3000015
Lipofectamine™ Stem Transfection Reagent	ThermoFisher Scientific	Cat# STEM00015
Luminata™ Crescendo Western HRP substrate, 100mL	ThermoFisher Scientific	Cat# 10776189
ProLong™ Gold Antifade Mountant with DAPI	ThermoFisher Scientific	Cat# P36935
Roche DIG Easy Hyb solution	Sigma-Aldrich	Cat# 11796895001
SpCas9, 1000 pmol	Synthego	N/A
Critical commercial assays		
CellTox™ Green Cytotoxicity Assay	Promega	Cat# G8742
Genomic DNA 165 kb Kit	Agilent	Cat# FP-1002-0275
hPSC Genetic Analysis Kit	STEMCELL Technologies	Cat# 07550
In-Fusion Snap Assembly Mix	Takara Bio	Cat# 638947
LightCycler® 480 SYBR Green mix	Roche	Cat# 04707516001
Monarch HMW DNA Extraction Kit for Cells and Blood	New England BioLabs	Cat# T3050
Nano-Glo® HiBiT Lytic Detection System	Promega	Cat# N3030
Nano-Glo® Live Cell Assay System	Promega	Cat# N2011
NEBNext® FFPE DNA Repair Mix	New England BioLabs	Cat# M6630
NEBNext® Quick Ligation Module	New England BioLabs	Cat# E6056
NEBNext® Ultra™ II End Repair/ dA-Tailing Module	New England BioLabs	Cat# E7546
Oxford Nanopore Technologies (ONT) Ligation Sequencing Kit V14	Oxford Nanopore Technologies	Cat# SQK-LSK114
Qiagen DNeasy Blood & Tissue Kit	Qiagen	Cat# 69504
QIAquick PCR Purification Kit	Qiagen	Cat# 28104
qPCR Lentivirus Titer Kit	Applied Biological Materials (abm)	Cat# LV900
Qubit dsDNA BR Assay Kit	ThermoFisher Scientific	Cat# Q32850
RNeasy extraction kit	Qiagen	Cat# 74104
Sequel II Sequencing Kit 3.2	PacBio	Cat# 102-194-100
SRE XS kit	PacBio	Cat# SKU 102-208-200
SuperScript™ IV Reverse Transcriptase	ThermoFisher Scientific	Cat# 18090050
Deposited data		
Long-read DNA sequencing of *C9orf72* repeats in DPReporter lines	This paper	Sequence read Archive (SRA) accession number: PRJNA1236332; https://www.ncbi.nlm.nih.gov/sra/?term=PRJNA1236332
Experimental models: Cell lines		
293T	ATCC	Cat# CRL-3216, RRID:CVCL_0063
C9orf72 patient iPSC	Ababneh et al., 2020[73]; Selvaraj et al., 2018[74]	N/A

(*Continued on next page*)

Continued

REAGENT or RESOURCE	SOURCE	IDENTIFIER
Experimental models: Organisms/strains		
D. melanogaster: UAS-36R(G4C2)	Mizielinska et al.[17]	N/A
Oligonucleotides		
ADAMTSL Fwd: CGGTGGCTCTATGGACTCG	This paper	N/A
ADAMTSL Rev: CAGGGGGATTAAAGGGCACAG	This paper	N/A
Fam83f Fwd: ACGTAGAGCCCTTTGACACG	This paper	N/A
Fam83f Rev: GGTATGAGGCAGTGCTCCTG	This paper	N/A
TRAM1 Fwd: CACATTCCTGCACGCTCG	This paper	N/A
TRAM1 Rev: AGACGATGTCCGCGTGATTC	This paper	N/A
HiBiT-C9orf72 Fwd: TGGCGGCTGTTCAAGAAGATT	This paper	N/A
HiBiT-C9orf72 Rev: AAGGAGACAGCTCGGGTACT	This paper	N/A
SNP rs10757668 Rev: AGCAATCTCTGTCTTGGCAAC	This paper	N/A
C9orf72 V1 Fwd: AGATGACGCTTGATATCTCCG	This paper	N/A
C9orf72 V1 Rev: GCAATCTCTGTCTTGGCAACAG	This paper	N/A
C9orf72 V1+3 Fwd: AGTTCCGCCCACGTAAAAGA	This paper	N/A
C9orf72 V1+3 Rev: GCAATCTCTGTCTTGGCAACAG	This paper	N/A
C9orf72 V2 Fwd: CGGTGGCGAGTGGATATCTCCGGAGC	This paper	N/A
C9orf72 V2 Rev: AGCAATCTCTGTCTTGGCAAC	This paper	N/A
C9orf72 V3 Fwd: GCAGGTGTGGGTTTAGGAGATATC	This paper	N/A
C9orf72 V3 Rev: GCAATCTCTGTCTTGGCAACAG	This paper	N/A
C9orf72 Total Fwd: GAGAGAATGGAAGATCAGGGTCA	This paper	N/A
C9orf72 Total Rev: TCTTCAGGAACACTGTGTGATTTCA	This paper	N/A
GAPDH Fwd: GAGTCAACGGATTTGGTCGT	This paper	N/A
GAPDH Rev: CCACTTGATTTTGGAGGGATCTC	This paper	N/A
ERN1 Fwd: AATTGTGTACCGGGGCATGT	This paper	N/A
ERN1 Rev: ACATACTCTTGCAGGGTGGC	This paper	N/A
DHX36 Fwd: ACCTGATGGAGCTGAACGCT	This paper	N/A
DHX36 Rev: AGCAGCAGAACAGTGCTCCA	This paper	N/A
DDX3X Fwd: CTTCGCGGTGGAACAAACAC	This paper	N/A
DDX3X Rev: GGTCTAGGCCAGCAAACTGC	This paper	N/A
Spliced *XBP1* Fwd: GCTGAGTCCGCAGCAGGT	This paper	N/A
Spliced *XBP1* Rev: CTGGGTCCAAGTTGTCCAGAAT	This paper	N/A
Total *XBP1* Fwd: TGAAAAACAGAGTAGCAGCTCAGA	This paper	N/A
Total *XBP1* Rev: CCCAAGCGCTGTCTTAACTC	This paper	N/A
Exon 1a_F: AGGTGCGTCAAACAGCGACAAGTTCCG	This paper	N/A
Exon 1b_F: GTTGCGGTGCCTGCGCC	This paper	N/A
Exon 4_R: CCATTACAGGAATCACTTCTCCAGTAAGCATTGG	This paper	N/A
Gene Knockout Kit v2 - human - ERN1 - 1.5 nmol	Synthego	N/A
Negative Control, Scrambled sgRNA#1, mod-sgRNA, 1 nmol	Synthego	N/A
Recombinant DNA		
pLKO.1 - TRC cloning vector	Addgene	Cat# 10878; RRID:Addgene_10878
psPAX2 plasmid	Addgene	Cat# 12260; RRID:Addgene_12260
pMD2.G	Addgene	Cat# 12259; RRID:Addgene_12259
pHAGE-DDX3X plasmid	Addgene	Cat# 116730; RRID:Addgene_116730
pHR-hSyn-EGFP plasmid	Addgene	Cat# 114215; RRID:Addgene_114215
pUltraHot-mCherry-DHX36-iso1-WT plasmid	Addgene	Cat# 206964; RRID:Addgene_206964

(*Continued on next page*)

Continued

REAGENT or RESOURCE	SOURCE	IDENTIFIER
Software and algorithms		
GraphPad Prism 8	GraphPad	RRID:SCR_002798
Harmony software	PerkinElmer	RRID:SCR_023543
Ilastik software	Berg et al., 2019	RRID:SCR_015246
Image Lab 6.1 software	Bio-Rad	RRID:SCR_014210
ImageJ	National Institutes of Health	RRID:SCR_003070
Long-read repeat sequence analysis code	This paper	https://doi.org/10.5281/zenodo.14996789
Other		
4D-NucleofectorTM and 96-well ShuttleTM System	Lonza	N/A
Amersham™ Imager 600	GE Healthcare Life Sciences	N/A
CellDiscoverer 7 imaging system	Zeiss	N/A
ChemiDoc XRS+ System	Bio-Rad	N/A
Echo® Acoustic Liquid Handler	Labcyte	N/A
FLUOstar® Omega Microplate Reader	BMG Labtech	N/A
ImageQuant™ LAS 4000	GE Healthcare	N/A
Incucyte®	Sartorius	N/A
LightCycler® 96 Instrument	Roche	N/A
Lonza™ P3 Primary Cell 4D-Nucleofector™ X Kit L	Lonza	Cat# 13429329
LSM880 confocal microscope	Zeiss	N/A
Opera Phenix™ Plus	PerkinElmer	N/A
Q800R3 Sonicator	QSonica	N/A
Trans-Blot Turbo Transfer System	Bio-Rad	N/A

EXPERIMENTAL MODEL AND STUDY PARTICIPANT DETAILS

iPSC lines

C9orf72 patient-derived iPSC lines used in this study have been previously reported: line M2IIR2 (male, ALS, ~638 repeats[73]); BS6 (C9 parental) (female, ALS/FTD ~700 repeats)[74]; BS6 isogenic control (female, 2 repeats)[74]; DN19 (male, ALS ~960 repeats).[74]

Drosophila

All experiments were conducted at 25°C on a 12 h:12 h light cycle at 60% humidity. For survival assays, female UAS-(GGGGCC)36 flies were crossed with elavGS males, and the eggs were collected and transferred into SYA-containing bottles at an equal density. Following eclosion, adult flies were allowed to mate for 48 h before the female flies were randomly allocated, under CO_2 anesthetization, to vials at a standard density (n = 15). Each vial contained SYA food media supplemented with RU486 (200 mM) and/or trametinib (15.6 μM), with EtOH and DMSO added as vehicle controls where appropriate. A minimum of 10 vials were used per treatment condition (n = 150). Three times a week, flies were transferred to new vials, and the number of dead or censored flies was recorded every one to two days. For survival assays two systems of drug administration were used. Non-delayed induction treatment groups were supplemented with both transgene inducer RU486 and trametinib/DMSO from day 0 (eclosion), thus inducing transgene expression throughout the experiment. Delayed induction groups received trametinib/DMSO supplemented SYA for the first seven days before the transgene was induced with RU486 for the remainder of the experiment. Log rank test on lifespan data were performed in Microsoft Excel (template available at http://piperlab.org/resources/) and data was plotted using Prism6.

METHOD DETAILS

Culturing and passaging of iPSCs

iPSCs were cultured on Geltrex (Gibco)-coated plates in Essential 8 medium (E8, Gibco) with daily media changes. Upon reaching ~80–90% confluency, cells were washed with 1xPBS (Gibco) and incubated in 500 μM EDTA (Gibco) for 3–4 min. After aspirating the supernatant, cells were lifted with 1 mL E8 medium, resuspended once, and distributed to new culturing plates. All cell lines were routinely karyotyped by an external provider (TDL Genetics) to verify genomic integrity. To further screen for karyotypic alterations after CRISPR/Cas9 genome editing, we used the qPCR-based hPSC Genetic Analysis Kit (STEMCELL Technologies).

Generation and induction of i^{3}Neurons

I^{3}Neuron cell lines were generated as described elsewhere.[37] Briefly, an expression cassette containing NLS-mApple and Tet-ON NGN2 was introduced into the CLYBL safe harbor locus by CRISPR/Cas9 genome editing. For induction into cortical neurons, iPSCs were lifted as single cells on day 0 with ACCUTASE (STEMCELL Technologies) and 5x10^5 cells per well were seeded onto Geltrex-coated 6-well plates in induction medium (DMEM:F12 Gibco (Thermo) 10565018, N2 supplement Gibco (Thermo) 17502048, non-essential amino acids Gibco (Thermo) 11140050, 10mM HEPES Gibco (Thermo) 15630056, Glutamax Gibco (Thermo) 35050061, 2μM Doxycycline Hyclate Sigma/Merck D9891, 10 μM ROCK inhibitor Y-27632 Miltenyi 130-103-922). Media was changed on days 1 and 2. On the third day, neural precursor cells (NPCs) were lifted with ACCUTASE and replated in maintenance medium (Neurobasal Gibco (Thermo) 12348017, B27 supplement Gibco (Thermo) 17504044, 10 ng/mL BDNF Gibco (Thermo) 10908-010, 10 ng/mL NT-3 Peprotech 450-03, 1 μg/mL laminin Merck Life Science L2020-1MG) onto poly-L-ornithine and laminin coated plates at the following densities: 5x10^5 cells/6-well plate, 5x10^4 cells/96-well plate, 1.5x10^4 cells/384-well plate. 96-well and 384-well plates were centrifuged for 5 s at 300xg to improve cell attachment and survival, before sealing with adhesive film (Greiner) to prevent edge effects. For long-term culturing, ½ media changes were performed every 3–4 days using maintenance medium.

CRISPR/Cas9 tagging of *C9orf72* DPRs

For tagging of endogenous DPRs with HiBiT, we designed single-guide RNAs (sgRNAs) to induce double-strand breaks 3′ of *C9orf72* exon 1b (AGGCGCAGGCGGTGGCGAGT, Synthego). Single-stranded DNA (ssDNA) donor templates were synthesized (Genscript) for selective tag integration into either the polyGA or polyGP frame. Lines were generated by introducing sgRNA, ssDNA, and recombinant SpCas9 (Synthego) into iPSCs through nucleofection with P3 Primary Cell 4D-Nucleofector X Kit L (Lonza). After clonal expansion, cell lines were characterised as described in the results section. To confirm reporter integration into the correct targeting site, PCR amplification of HiBiT-*C9orf72* (forward primer: TGGCGGCTGTTCAAGAAGATT; reverse primer: AAGGAGACAGCTCGG GTACT) was performed using DreamTaq 2x Mastermix (ThermoFisher) according to the manufacturer's instructions. To determine whether integration had occurred in the expanded allele, RNA was extracted from reporter lines using the RNeasy extraction kit (Qiagen) before reverse transcription with SuperScript IV Reverse Transcriptase (Invitrogen). To detect the SNP rs10757668 in reporter-containing transcripts, we used a forward primer located in the reporter sequence (TGGCGGCTGTTCAAGAAGATT) and a reverse primer in exon2 (AGCAATCTCTGTCTTGGCAAC). cDNA was amplified by PCR, extracted using QIAquick PCR Purification Kit (Qiagen), and sequenced by an external provider (Source Bioscience) to identify the SNP.

MSD immunoassay

Detection of polyGA and polyGP by MesoScale Discovery (MSD) immunoassay was performed as previously described.[38,39]

RNA-FISH for sense and antisense foci

For RNA fluorescent *in situ* hybridization (RNA-FISH) in i^{3}Neurons, 25,000 NPCs were seeded per well in 96-well plates and treated with periplocin EC97.50 or DMSO (N = 3 neuronal inductions per line). After 72 h, cells were fixed in 4% PFA (PBS-diluted) for 7 min, dehydrated in 70% and 100% ethanol, and stored at −80°C in 100% ethanol until further use. Cells were then rehydrated in 70% ethanol, washed in pre-hybridization buffer (40% formamide, 2× SSC, 10% dextran sulfate, 2 mM vanadyl ribonucleoside complex) for 5 min at room temperature, and permeabilized with 0.2% Triton X-100 in PBS for 10 min. Following a 30-min blocking step at 66°C in pre-hybridization buffer. Digoxigenin (DIG)-labelled locked nucleic acid (LNA) probes (Qiagen) were used to detect either sense (/5DIG/CCCCGGCCCCGGCCCC/3DIG/) or antisense (/5DIG/GGGGCCGGGGCCGGGG/3DIG/) RNA foci. Alternatively, LNA probes directly labeled with a fluorescent dye were used for RNA-FISH of sense (5′ TYE563-labelled CCCCGGCCCCGGCCCC) or antisense foci (5′ TYE563-labelled GGGGCCGGGGCCGGGG) in iPSCs (Figure S3). Briefly, probes (40 nM, pre-hybridization solution) were denatured at 95°C for 10 min and hybridization was then carried out in the dark at 66°C for 3 h, allocating separate wells for either sense or antisense probes. Post-hybridization, cells were washed sequentially in 0.2% Triton X-100 in 2× SSC (5 min, room temperature) and in 0.2× SSC (30 min, 66°C, followed by 20 min, 66°C). DIG-labelled probes were detected using a 488-conjugated DIG antibody (Vector Laboratories, DI-7488-.5, 1:1000 in 0.2× SSC with 1% BSA) incubated overnight at 4°C, followed by a 20-min wash in 0.2× SSC at room temperature. Nuclei were counterstained with Hoechst (1 μg/mL in 0.2× SSC) for 10 min. Cells were maintained in 0.2× SSC at 4°C, protected from light. Imaging was performed using the Opera Phenix high-content system (PerkinElmer) with a 40 ×1.1 NA objective. RNA foci were detected and quantified using Harmony software (PerkinElmer). A nuclear mask was generated based on the Hoechst signal, and the percentage of cells containing at least one RNA focus within the nucleus was calculated for each condition.

Off-target sequencing and genetic integrity

We used the Off-Spotter tool[75] to determine the 3 coding regions with the highest risk of off-target cutting by the sgRNA used for CRISPR editing. The genes (*ADAMTSL5*, *Fam83f*, *TRAM1*) were amplified by qPCR (primers sequences provided in Key Resources Table) and sequenced by an external provider (Source Bioscience). To determine presence of the most common karyotypic abnormalities by qPCR, we utilized the hPSC Genetic Analysis Kit (Stemcell Technologies) according to manufacturer's instructions.

Karyotyping

Karyostat+ whole-genome chromosomal microarray karyotyping was performed by ThermoFisher.

Long-read sequencing

Genomic DNA was extracted using the Monarch HMW DNA Extraction Kit for Cells and Blood (New England BioLabs, T3050) following the manufacturer's instructions. The DNA quality, quantity and size distribution were assessed using a Qubit fluorometer with the Qubit dsDNA BR Assay Kit (Thermo Fisher Scientific, Q32850) and a Femto Pulse system with the gDNA 165 kb analysis kit (Agilent Technologies, FP-1002-0275).

PacBio sequencing

Library preparation and sequencing were conducted using the PacBio PureTarget method (#103-329-400, REV02). Briefly, DNA ends were dephosphorylated to prevent adapter ligation to non-targeted DNA ends. Cas9 gRNA complexes were formed using the repeat expansion panel, ahead of dsDNA digestion at targeted regions. dA tails were added to DNA 3′ ends, the indexed SMRTbell adapters were ligated to the targeted DNA fragments. DNA fragments that had not formed SMRTbell templates were removed by nuclease treatment. Samples were pooled and cleaned up using SMRTbell cleanup beads. The pooled SMRTbell templates were washed with SMRT boost beads, then concentrated with SMRTbell cleanup beads. The sequencing primer was then annealed, the sequencing polymerase bound, and the complexes purified with SMRTbell cleanup beads. The final library was sequenced on the PacBio Sequel II system using the Sequel II Binding Kit 3.2 and the Sequel II Sequencing Kit 3.2 (PacBio, 102-194-100). Bioinformatics analysis was performed in R using a custom script available at https://github.com/mike-flower. Circular consensus sequences (CCS) were filtered for quality and then aligned to the *C9orf72* reference sequence (NCBI, 203228) using rBLAST. Reads were split into flanking and repeat sequences. Waterfall plots were generated using ggplot2. Reads were clustered by repeat length using factoextra and NbClust, then consensus sequences were generated using the msa package.

Nanopore adaptive long-read sequencing

A protocol for sample preparation and nanopore processing was developed by the Genomics England Scientific R&D Team with some minor modifications. 6–6.4 μg of DNA was fragmented to 10–15 kb using Covaris g-TUBEs (520079, Covaris). Samples were centrifuged using an Eppendorf 5424 (022620401, Eppendorf) centrifuge for 1 min at 4500–4800 rpm, rotated 180° and centrifuged for a further minute at 4500–4800 rpm. Fragments under 5 kb were reduced using the SRE XS kit (SKU 102-208-20,0 PacBio). An equal volume of Buffer SRE-XS was added to the fragmented DNA sample and centrifuged at 10,000 xg for 30 min before discarding the supernatant. The DNA pellet was washed with 200 μL of 70% ethanol for a total of two ethanol washes. The remaining ethanol was evaporated off at 37°C for 2–15 min as required. 50 μL of PacBio Buffer EB was used to resuspend the pellet at 37°C for 10–20 min then 4°C overnight. For library preparation 1–1.5 μg of sample in 48 μL of nuclease-free water (NFW) was mixed with 3.5 μL NEBNext FFPE DNA Repair Buffer, 3.5 μL Ultra II End-Prep Reaction Buffer, 2 μL NEBNext FFPE DNA Repair Mix (M6630, NEB) and 3 μL Ultra II End-Prep Enzyme Mix (E7546, NEB) and incubated at 20°C for 10 min followed by 65°C for 10 min. The reaction was then incubated at room temperature for 10 min on a hula mixer with 60 μL of AMPure XP Beads (A63881, Beckman Coulter). The beads were pelleted on a magnet and washed with 200 μL of 70% ethanol twice before eluting in 64 μL NFW at room temperature for 10–30 min. The library was processed using Oxford Nanopore Technologies (ONT) Ligation Sequencing Kit V14 (SQK-LSK114). 62 μL of eluted DNA was added to a mix of 25 μL ONT Ligation Buffer, 8 μL NEBNext Quick T4 DNA Ligase (E6056, NEB) and 5 μL ONT Ligation Adapter and incubated at room temperature for 30 min. 40 μL of AMPure XP beads were added and incubated on a hula mixer at room temperature for 10 min then pelleted on a magnet. The beads were washed twice with 250 μL ONT Long Fragment Buffer then eluted in 34 μL ONT Elution Buffer at 37°C for 15 min. 10–15 fmol of library was loaded onto a single PromethION Flow Cell (R10.4.1) following manufacturer's instructions. Adaptive sampling was carried out as described below. The run lasted 72 h with two 1-h nuclease flushes between 20-24 h and 44–48 h using the ONT Flow Cell Wash Kit (EXP-WSH004) following manufacturer's instructions. The library was stored at 4°C during the run and 10–15 fmol of library was loaded after each nuclease flush. For adaptive sampling and analysis, all code can be found at: https://github.com/rainwala/GIU-rep_exp_blast_finder. Adaptive Sampling was carried out using the Adaptive Sampling option on MinKnow version 24.02.10. The reference genome used was GRCh38.p14 (https://www.ncbi.nlm.nih.gov/datasets/genome/GCF_000001405.40/) and the co-ordinates were specified in bed format as follows: chr9 27543537 27603536 C9orf72_expansion_region. This corresponds to the file C9orf72_adaptive.bed in the Github repository above. Once sequencing was complete, the nextflow process rep_exp_blast_finder.nf was run on the sequencing output to generate the final output.

DPR-HiBiT lytic detection assay

For the detection of DPR-HiBiT, the Nano-Glo HiBiT Lytic Detection System (Promega) was used. In short, Nano-Glo HiBiT Lytic Buffer was brought to room temperature before adding LgBiT protein 1:100 and Nano-Glo HiBiT detection reagent 1:50. The solution was mixed and added to culturing plates in a 1:1 ratio. Reactions were incubated on an orbital shaker for 10 min at 600 RPM. Luminescent signals were quantified with a PHERAstar Microplate Reader (BMG Labtech).

DPR-HiBiT live cell assay

To detect DPR-HiBiT in live cells, a plasmid encoding LgBiT (Promega) was introduced into NPCs on day 3 of the differentiation protocol by nucleofection with the P3 Primary Cell 4D-Nucleofector X Kit S (Lonza). 3 days after nucleofection, we used the Nano-Glo Live Cell Assay System (Promega). Briefly, Nano-Glo LCS Dilution Buffer was brought to room temperature before adding Nano-Glo Live Cell Substrate 1:1:20. The solution was mixed and added to culturing plates in a 1:1:4 ratio. Plates were incubated on an orbital shaker for 15 s at 400 RPM. Luminescent signals were quantified with a PHERAstar Microplate Reader (BMG Labtech).

DPR-HiBiT live labeling

For live-labelling of endogenous DPRs, DPReporter cell lines were transduced with lentivirus containing a Tet-ON-LgBiT cassette to generate a stable cell line with inducible LgBiT expression. After clonal expansion and screening to identify successfully edited clones, cells were induced into NPCs as described. On the third day of differentiation, cells were seeded onto 96-well plates in maintenance media with doxycycline. After culturing cells overnight at 37°C, we used the Nano-Glo Live Cell Assay System (Promega) as described to detect baseline luminescence. Thereafter, all media was removed, and cells were washed with 1x PBS before adding new maintenance media without doxycycline. Detection of labeled DPRs by Nano-Glo Live Cell Assay was repeated on days 1, 3, 5, and 7 after replating.

Small molecule screening workflow

Small molecule pilot screening was performed using a natural product library (MedChemExpress) comprising 1,444 molecules. All compounds were transferred to 384-well plates with an Echo Acoustic Liquid Handler (Labcyte) and screened at a final concentration of 10 μM. Cells were induced as described until day 2 of the differentiation protocol. On day 2, assay plates, containing the library, were brought to room temperature, and coated with 10 μg/mL laminin in 12.5 μL maintenance medium for 2 h at 37°C. Thereafter, DPReporter NPCs were lifted, washed, and counted as described before seeding $1.5x10^4$ cells/well in maintenance medium by adding a further 12.5 μL onto the coating solution. Plates were centrifuged for 5 s at 300xg, sealed with EasySeal plate sealer (Greiner), and cultured at 37°C for 72–120 h. On the experimental day, plates were brought to room temperature for 30 min before adding 5 μL of previously prepared CellToxGreen (Promega) solution. Plates were centrifuged for 5 s at 300xg, incubated on an orbital shaker (200 RPM, 5 min), and fluorescence was quantified using a PHERAstar Microplate Reader (BMG Labtech). Thereafter, 25 μL previously prepared Nano-Glo HiBiT Lytic Detection solution was added to each well followed by centrifugation for 5 s at 300xg, incubation on an orbital shaker (400 RPM, 10 min), and quantification of luminescent signal (PHERAstar Microplate Reader, BMG Labtech). We identified toxic compounds by calculation of the 3xSD window of DMSO control wells and excluded every molecule outside of this range. Similarly, we defined hit compounds amongst the remaining molecules by DPR-HiBiT signals greater or smaller than the mean ± 3xSD of DMSO control wells.

CRISPR screen workflow

CRISPR knockout (CRISPRn) screening was performed using an arrayed screening library for all human helicases (Synthego) containing three sgRNAs per well. The sgRNA library was resuspended in TE buffer as instructed by the manufacturer and transferred to 96-well format (3 μL, 5μM) for storage. On the day of screening, the 96-well library plates were thawed on ice, 0.25 μL recombinant SpCas9 (Synthego, 20 μM) was added to each well before centrifugation for 1 min at 300xg to induce the formation of RNP complexes. Plates were incubated at room temperature in a sterile hood while 3-day-old NPCs were washed with 1x PBS and lifted with ACCUTASE as described. $2x10^5$ cells per CRISPR reaction were collected, centrifuged, and resuspended in P3 nucleofection solution (Lonza). Using a multichannel pipette, 21.5 μL of the cell solution was transferred to the RNP complexes and resuspended 3–4 times. Then, 23 μL of the RNP-cell mixture were transferred to 96-well Nucleocuvette Plates (Lonza) and nucleofected with a 4D-Nucleofector and 96-well Shuttle System (Lonza), using program CA137. After nucleofection, 77 μL maintenance medium was added to each well before incubation at 37°C for 10 min to improve cell viability. Cells were then equally split between PLO/laminin-coated 96-well assay and imaging plates for primary and secondary screening, respectively, before centrifugation for 5 s at 300xg. After 3 days, primary screening was performed by subsequently performing the CellToxGreen Cytotoxicity assay (Promega) and the Nano-Glo HiBiT Lytic Detection System (Promega). We identified toxic genome editing events as differing by > 3xSD of control wells with non-targeting sgRNAs in the toxicity assay. Similarly, we defined hit genes by DPR-HiBiT signals lower than the mean -3xSD of control wells.

Secondary screening workflow

To determine changes in global translation rates, we quantified the expression of a canonically translated NLS-mApple reporter. A CellDiscoverer 7 imaging system (Zeiss) was used to image 5% (96-well) or 20% (384-well) of each well with 40× magnification. We then generated a custom image-analysis pipeline by machine learning (ilastik).[76] Quantification masks were generated using pixel classification, to distinguish fluorescence and background signals. Binary segmentation masks were exported and combined with fluorescent images (quantification mask) for processing in Ilastik by pixel and object classification. Objects are detected using the quantification mask and fluorescent intensities per object were measured.

Pathway analysis

STRING analysis was performed by determining functional and physical protein association at the highest (0.900) or medium (0.400) confidence for all helicases and hit genes, respectively. After identifying a potential enrichment of telomere-associated helicases, we mined the available literature of every helicase for telomere-regulating activity, identifying further hit and non-hit genes to be associated with telomeres. The entirety of genes identified by STRING and literature mining was used to calculate pathway enrichment (Fisher's Exact Test).

RT-qPCR

RNA was extracted from cultured cells using the RNeasy extraction kit (Qiagen) before reverse transcription with SuperScript IV Reverse Transcriptase (Invitrogen) according to the manufacturer's instructions. QPCR was then performed using the LightCycler 480 SYBR Green mix (Roche) on a LightCycler 96 Instrument (Roche) and quantified using the 2-ddCT-method. Primer sequences provided in Key Resources Table.

Assay for quantification of exon1a/1b usage

RNA was extracted from all iPSC DPReporter lines using the RNeasy extraction kit (Qiagen) before reverse transcription with SuperScript IV Reverse Transcriptase (Invitrogen). To detect exon 1a and exon 1b, we used specific forward primers for each exon along with a common reverse primer located on exon 4 (Exon 1a_F: AGGTGCGTCAAACAGCGACAAGTTCCG; Exon 1b_F: GTTGCGGTGCCTGCGCC; Exon 4_R: CCATTACAGGAATCACTTCTCCAGTAAGCATTGG), which produced amplicons of sufficient size for subsequent next-generation sequencing. PCR reactions (30 cycles) with the exon 1a and exon 1b forward primers, both paired with the exon 4 reverse primer, were performed in separate tubes and then combined in a single tube and column purified (Qiagen). Sequencing was performed by Plasmidsaurus using Oxford Nanopore Technology. FASTQ files were aligned to the sequence constructed from *C9orf72* exons 1a, 1b, and 2 using minimap2[77] with long-read splice-aware alignment parameters (-x splice). Coverage analysis was performed by intersecting BAM files with a BED file containing exon coordinates using bedtools.[78] The number of reads overlapping each exon, and the percentage of total mapped reads were computed.

Immunocytochemistry

Cells were cultured on coated coverslips and fixed with 4% Paraformaldehyde for 10 min at room temperature. After washing with 1x PBS, cells were blocked with 5% BSA in 0.3% PBS-TritonX for 1 h at room temperature. Primary antibodies GABAA Receptor (α1 subunit) 1:100 Sigma (G4416); GluR2 1:100 ThermoFisher (32–0300); Map2 1:500 Millipore (MAB3418); OCT4 1:2000 Cell Signaling (2750); SOX2 1:100 Cell Signaling (35795); TuJ1 1:500 Cell Signaling (5568T) were diluted in 5% BSA in PBS and added to samples for overnight incubation at 4°C. On the next day, cells were washed 3x for 5 min with 0.3% PBS-T before adding secondary antibodies (goat anti-mouse IgG2a Alexa Fluor 488 1:1000 Invitrogen (A21131); donkey anti-rabbit IgG Alexa Fluor 488 1:1000 BioLegend (406416); goat anti-rabbit IgG Alexa Fluor 546 1:1000 ThermoFisher (A11035)) in blocking solution. Samples were washed again before mounting coverslips with ProLong Gold Antifade Mountant with DAPI (Thermo Fisher). Images were taken on an LSM880 confocal microscope (Zeiss) and analyzed in ImageJ.

Western blotting

Cells were washed with PBS before harvesting in lysis solution: RIPA, 2% SDS, 2x Protease inhibitor (cOmplete, Mini Protease Inhibitor Cocktail, Roche). Samples were sonicated using a Q800R3 Sonicator (QSonica) before centrifugation for 20 min at 17,000xg to remove debris. The supernatant was transferred, and protein concentration was determined by Pierce BCA (ThermoFisher) before loading equilibrated samples on 4–12% NuPAGE Bis Tris gels (ThermoFisher). Blots were transferred to nitrocellulose membranes using the Trans-Blot Turbo Transfer System (Bio-Rad). Membranes were blocked for 1 h at room temperature before incubation with primary antibodies: AMPK alpha-1,2 1:1000 ThermoFisher (PA5-36045); C9orf72 1:1,000 GeneTex (GTX634482); eIF2α 1:100 Cell Signaling Technology (D7D3), #62928; ERCC8 1:100 Abcam (ab137033); ERK1/ERK2 1:1000 ThermoFisher (13–6200); GAPDH (14C10) 1:5000 Cell Signaling Technology (#2118); phospho-eIF2α 1:100 Cell Signaling Technology (D9G8), #3398; phospho-ERK1/ERK2 1:1000 ThermoFisher (MA5-33180); phospho-PKR 1:500 Abcam (AB32036); PKR 1:500 Abcam (AB32506); RECQL 1:100 Abcam (AB150421); RECQL4 1:100 Abcam (AB188125); RTEL1 1:100 Proteintech (25337-1-AP); UPF1 1:1000Proteintech (66898-1-Ig); XBP1s 1:100 Cell Signaling Technology (D2C1F), #12782 in blocking solution overnight at 4°C. On the next day, blots were washed 5 × 5 minutes before incubation with secondary antibodies (goat anti-mouse HRP 1:10000 ThermoFisher (31430); goat anti-rabbit HRP 1:10000 ThermoFisher (31460)) for 1 h at room temperature. After further 5 × 5 minute washes, blots were imaged on an Amersham Imager 600 (GE Healthcare Life Sciences) and quantified using ImageJ.

For *Drosophila* protein extraction, 10 heads per replicate were homogenized in 12.5% trichloroacetic acid (TCA) (Merck) and centrifuged for 15 min at 13,000 rpm at 4°C. The pellet was washed with 1M Tris and resuspended in NuPAGE LDS Sample Buffer (4x) (Thermo Fisher) containing 100 mM DTT. Proteins were denatured for 15 min at 90°C and separated on NuPAGE 4–12% Bis-Tris precast gels (Thermo Fisher) using MES Running Buffer (Life Technologies). Proteins were transferred to PVDF membranes, which were blocked in Tris-buffered saline (TBS) containing 0.05% Tween 20 (TBS-T) and 5% BSA for 1 h at room temperature. Membranes were then incubated overnight at 4°C in blocking buffer containing the diluted primary antibodies. The following primary antibodies were used: phospho-Erk (Thr202/Tyr204) (Cell Signaling, 4370, 1:2000), total-Erk (Cell Signaling, 4695, 1:2000), anti-polyGP[17]

(1:2500), and α-tubulin (Merck, T6199, 1:2000). Membranes were then washed three times for 5 min with TBS-T and probed with secondary antibody (anti-rabbit HRP (ab6721) or anti-mouse HRP (ab6789), Abcam, 1:10,000) in TBS-T for 1 h at room temperature, followed by three washes with TBS-T for 5 min each. Blots were imaged using Luminata Crescendo (Millipore) and the ImageQuant LAS 4000 system. Quantification analysis of blot images was carried out using Fiji software.

Antisense oligonucleotide treatment of i^{3}Neurons

Cells were induced into neural precursor cells and replated on day 3 of the protocol as described above. For standard treatments, ASOs (*C9orf72* intron upstream of repeat: 5'-mU*mA*mC*mA*mG*G*C*T*G*C*G*G*T*T*G*mU*mU*mU*mC*mC- 3'; non-targeting 5′-mC*mC*mU*mU*mC*C*C*T*G*A*A*G*G*T*T*mC*mC*mU*mC*mC- 3'; m = 2′O-methyl RNA bases.

* = phosphorothioate) were added to culturing media directly at concentrations between 1 μM and 10 μM with ½ media changes every 3–4 days. For improved treatments, 0.4 μL Lipofectamine Stem (Thermo) reagent and ASOs were mixed in a reaction tube with 50 μL Opti-MEM for 10 min at room temperature and added to 96-wells with replated i^{3}Neurons. The medium was replaced by maintenance medium supplemented with ASOs after 4 h.

Cloning of lentiviral transfer plasmids

The cDNA sequences for DDX3X and DHX36 were individually PCR-amplified from their respective plasmids, sourced from Addgene (#116730; #206964). Following amplification, each cDNA was cloned into the pHR-hSyn-EGFP lentiviral backbone (Addgene #114215) using In-Fusion cloning (Takara Bio, #638947) at the BamHI and NotI sites, effectively replacing the EGFP cDNA in the backbone. For control experiments, the original unmodified pHR-Syn-EGFP was utilized. For the lentivirus-mediated gene knockdown study, shRNAs targeting DDX3X (clone ID: TRCN0000000001) and DHX36 (clone ID: TRCN0000050705) were inserted into the lentiviral plasmid backbone pLKO.1 (Addgene #10878) using annealed oligo cloning with AgeI and EcoRI restriction sites.

Lentiviral production and transduction

Low passage HEK293T cells were cultured in DMEM supplemented with 10% FBS, 4.5 g/L glucose, 110 mg/L sodium pyruvate, and 1x GlutaMAX. The cells were seeded in T175 flasks at 50% confluency 24 h before transfection. Transfection was performed with 14.1 μg of 2nd generation lentiviral packaging plasmid PAX (Addgene #12260), 9.36 μg of VSV-G envelope expressing plasmid (Addgene #12259), and 14.1 μg of the lentiviral transfer plasmid of interest, using Lipofectamine 3000 Transfection Reagent (Invitrogen) following the manufacturer's instructions. 48 h post-transfection, the cell media was harvested and centrifuged at 500xg at 4°C for 10 min to remove cell debris, then incubated overnight at 4°C with Lenti-X concentrator (Clontech) at a 3:1 media to concentrator ratio. The mixture was centrifuged at 1500xg at 4°C for 45 min, and the resulting concentrated lentiviral pellet was resuspended in sterile PBS, aliquoted, and stored at −80°C for future use. The lentiviral titer was measured using the Applied Biological Materials (abm) qPCR Lentivirus Titration Kit (#LV900) as per the manufacturer's instructions. A physical titer of 2–3 x 10^8 IU/mL was used to transduce i^{3}N DPReporter lines (72 h after initiating neural induction), with the vector volume constituting one-tenth of the total cell culture volume. 4.5 days after transduction, neuron counts were performed using the Incucyte (Sartorius) just before the HiBiT assay. Fluorescence signal from the NLS-mApple cassette integrated into i^{3}N DPReporter lines was imaged and the Incucyte 2023A software used to identify and quantify nuclei. This enabled normalization of the HiBiT signal to cell number, as shown in Figures S12K and S13.

CRISPR-Cas9 mediated ERN1-knockdown

Three sgRNAs from the ERN1 Gene Knockout Kit v2 (Synthego) or a non-targeting control sgRNA (Synthego, scrambled sgRNA#1) were pre-incubated at room temperature for 20 min with recombinant SpCas9 protein (Synthego) at a 8:1 sgRNA:SpCas9 molar ratio. 48 h after initiating neural induction, 8x10^5 i^{3}N GA-HiBiT cells were nucleofected in 100 μL single cuvettes with sgRNAs (300 pmol) and SpCas9 protein (36 pmol) using the P3 Primary Cell 4D-Nucleofector X Kit L (Lonza). Subsequently, cells were cultured in induction media in 12-well plates for RT-qPCR and ICE analysis (Synthego), or in 96-well plates for the HiBiT assay and luminescence signal was normalised to cell number as described above.

Southern blotting

Genomic DNA was extracted from the DPReporter lines using the Qiagen DNeasy Blood & Tissue Kit (Qiagen, cat #69504) as per the manufacturer's protocol. Southern blot analysis of the repeat size was undertaken as previously described[2] with some minor modifications. Genomic DNA was digested with Alu1/DdeI overnight at 37°C and 12 μg was electrophoresed on a 0.8% agarose gel alongside the DIG-labelled DNA molecular weight marker VII (Sigma-Aldrich, cat#11669940910). The DNA was transferred overnight to a positively charged nylon membrane (Sigma-Aldrich, cat #1141724001) by capillary blotting and was crossed-linked the following morning by UV. The membrane was prehybridized in Roche DIG Easy Hyb solution (Sigma-Aldrich, cat#11796895001) with the addition of 100ug/ml denatured salmon sperm (Thermo, cat#15632011) for 3 h at 48°C. The membrane was probed overnight at 48°C with 10 ng/ml of a DIG labeled oligonucleotide comprising of five hexanucleotide repeats (GGGGCC)5 (Integrated DNA technologies). Following hybridization, the membrane was first washed in a 2x sodium citrate (SSC) and 0.5% sodium dodecyl sulfate for 15 min while the hybridization oven ramped from 48°C to 65°C. The membrane was then further washed in 2x SSC and 0.5% SDS for 15 min, followed by 15 min washes in 0.5X SSC and 0.5% SDS and 0.15X SSC and 0.5% SDS. Antibody detection was carried

out following the DIG Application Manual protocol (Roche Applied Science) using the DIG wash and block buffer set (Roche, cat #11585762001) and ready-to-use CSPD (Sigma-Aldrich, cat#11755633001). Signals were visualised using ChemiDoc XRS+ system (BioRad). Membranes were exposed for 45 min with images collected every 4–5 min. Hexanucleotide repeat expansions were sized using Image Lab 6.1 software (BioRad) by comparison to DIG-labelled DNA molecular weight marker VII and subtraction of the genomic non repeat region of C9 flanking the AluI/DdeI restriction cut sites (156 bp).

QUANTIFICATION AND STATISTICAL ANALYSIS

Statistical tests were performed using GraphPad Prism. A t test was used for comparing two groups and ANOVA for more than two groups. The specific test used can be found in the figure legends describing the data. Fly lifespan experiments were analyzed using a log rank test.